Animal model

Xenograft experiments were performed as previously described [20]. Briefly, control or *GLI2* shRNA-transfected 143B cells (1×10^6) were suspended in 100 µl Matrigel (BD, NJ, USA). Cell suspensions were subcutaneously inoculated in 5 week-old nude mice. Tumour size was calculated weekly, using the formula $LW^2/2$ (where L and W represent the length and width of the tumour). Mice were randomly treated with GANT61 (50 mg/kg) or an equal volume of DMSO as control. GANT61 or DMSO was also injected subcutaneously. Injection of GANT61 started 1 week after inoculation of 143B cells. Treatments with GANT61 or DMSO were performed every other day. All animal experiments were performed in compliance with the guidelines of the Institute of Laboratory Animal Sciences, Graduate School of Medical and Dental Sciences, Kagoshima University. Every effort was employed to minimize the number of animals used and animal pain.

Cell cycle analysis

Cells were harvested with trypsin–EDTA. The cells were rinsed with PBS, fixed with 70% ethanol for 2 hr at 4 °C, washed three times with cold PBS and resuspended with 500 µL staining buffer containing PBS, pH 7.4, RNase A and 50 µg/ml propidium iodide (Wako). DNA content was examined by flow cytometry, using FACS Vantage SE (Becton-Dickinson, Franklin Lakes, NJ, USA) or CyAn™ ADP (Beckman Coulter, CA, USA) with FlowJo software (Tree Star) and Summit software (Beckman Coulter), respectively.

Statistical analysis

All experiments were performed three times unkess otherwise stated, and samples were analysed in triplicate. Results are presented as mean (SD). The statistical difference between groups was assessed by applying Student's t-test for unpaired data, using Microsoft Office Excel (Microsoft, Albuquerque, NM, USA) and Statistica (StatSoft, Tulsa, OK, USA).

Results

Activation of Hedgehog pathway in human osteosarcoma

We previously reported that several genes of the Hedgehog pathway were increased in five osteosarcoma cell lines and nine osteosarcoma biopsy specimens [21]. In the present study, we examined the expression of *SMO*, *PTCH1* and *GLI2* in three additional osteosarcoma biopsy tissues. We found that *SMO* expression was up-regulated in all osteosarcoma patient tissues, from 7.3- to 183-fold (Figure 1A). Similarly, the expression of *PTCH1* and *GLI2* was up-regulated in all three biopsy samples, from 8.6- to 72.3-fold and from 1.6- to 45.6-fold, respectively (Figure 1A). In agreement with these results, recombinant Sonic Hedgehog activates a reporter gene carrying $8 \times 3'$ Gli-BS–δ51LucII (GLI–Luc) in 143B and Saos-2 human osteosarcoma cells (Figure 1B) [17,18]. These findings corroborate our previous findings and indicate that the Hedgehog pathway is active in human osteosarcoma [21].

Inhibition of GLI prevents osteosarcoma cell proliferation

To examine the effects of GLI inhibition, we used GANT61, a pharmacological agent known to effectively block GLI transcription [22]. The MTT assay revealed that GANT61 dose-dependently inhibited the proliferation of 143B, Saos-2 and HOS cells (Figure 2A–C). In contrast, the same concentration of GANT61 did not affect the proliferation of normal human osteoblasts (NHOst) (Figure 2D). These findings suggest that inhibition of GLI prevents osteosarcoma proliferation *in vitro*.

Knockdown of *GLI2* prevents osteosarcoma proliferation *in vitro*

In order to evaluate the function of GLI in osteosarcoma, we knocked down GLI expression by using siRNA; scrambled siRNA was used as a negative control. MTT assay revealed that knockdown of *GLI1* did not affect the osteosarcoma cell proliferation (data not shown). On the other hand, MTT assay showed that knockdown of *GLI2* inhibited the proliferation of 143B and Saos-2 cells (Figure 3B). To rule out the possibility of an artifact due to off-target effects, we transfected the cells with two other shRNA sequences and obtained results comparable to those observed with *GLI2* siRNA (data not shown). We next examined the effects of *GLI2* knockdown on anchorage-independent osteosarcoma growth. The colony formation assay revealed that knockdown of *GLI2* reduced the number of colonies formed in soft agar (Figure 3C). These findings revealed that *GLI2* knockdown inhibits osteosarcoma growth.

GLI2 knockdown prevents cell cycle progression of human osteosarcoma cells

We next examined the role of GLI2 in the regulation of cell cycle. In 143B cells, following *GLI2* knockdown by *GLI2* shRNA, the proportion of cells in G_1 phase increased from 74.2% to 80.4% (Figure 4A). In Saos-2 cells, following *GLI2* knockdown by *GLI2* shRNA, the proportion of cells in G_1 phase increased from 60.5% to 68.7% (see Supporting information, Figure S1A), indicating that knockdown of *GLI2* promoted cell cycle arrest. We further examined the expression of cell cycle-related genes. Real-time PCR revealed that knockdown of *GLI2* decreased the expression of cell cycle accelerators, such as *cyclin D1* and

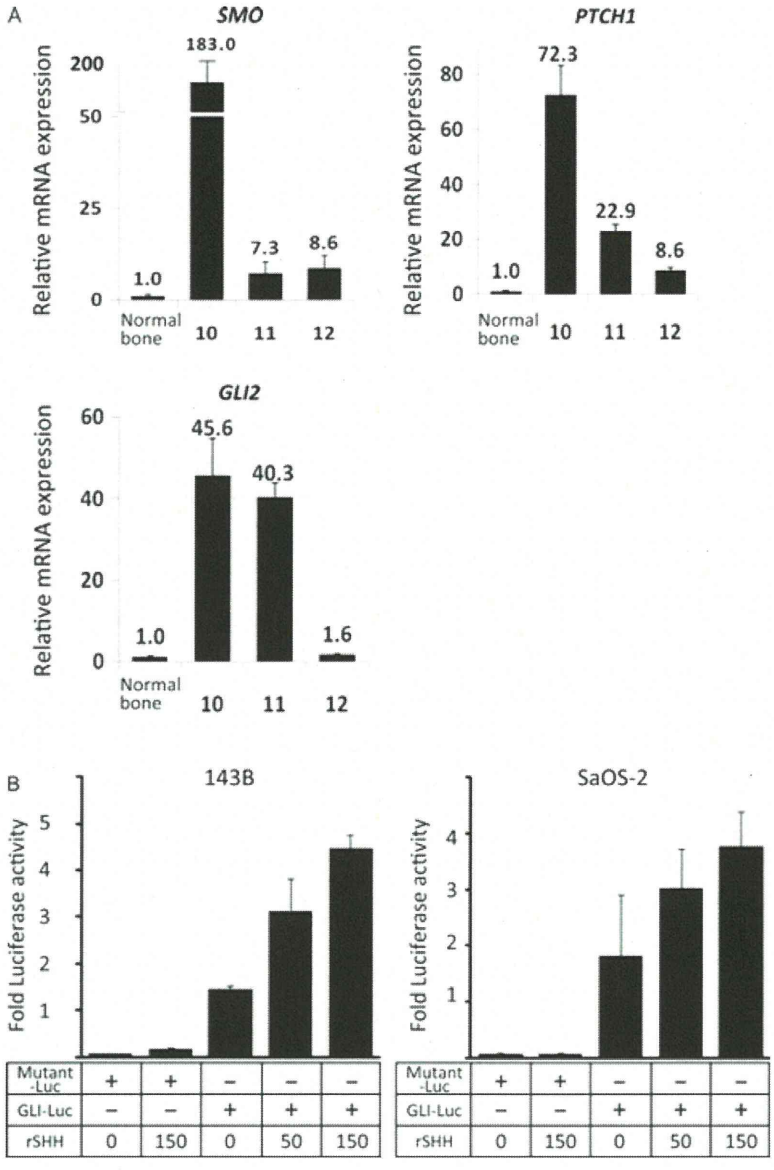

Figure 1. Activation of the Hedgehog pathway in human osteosarcoma. (A) Total RNA obtained from osteosarcoma biopsy tissues was examined by real-time quantitative PCR. Comparative Ct ($^{\Delta\Delta}$ Ct) analysis was performed to evaluate fold changes of mRNA expression using *GAPDH* or *ACTB*. All three human osteosarcoma biopsy specimens showed increased expression of *SMO* (7.3–183.0-fold), *PTCH1* (8.6–72.3-fold) and *GLI2* (1.6–45.6-fold). (B) 143B and Saos-2 cells were co-transfected with 8 × 3′ Gli-BS–δ51LucII (GLI–Luc), 8 × m3′ GLI-BS–δ51LucII (mutant-Luc) and internal control luciferase vector. The cells were treated with recombinant sonic hedgehog (rSHH). The luciferase activity was analysed after 24 h transfection and normalized to internal control luciferase activity. Values represent mean ± SD ($n = 3$).

SKP2 (Figure 4B). In mammals, cell cycle regulators are short-lived proteins that are regulated by protein degradation. Western blot analysis further confirmed that knockdown of *GLI2* decreased the protein levels of cyclin D1, pRb and SKP2 (Figure 4C). We next examined the expression of $p21^{cip1}$, a negative regulator of cell cycle progression. Western blot analysis revealed that $p21^{cip1}$ was up-regulated following knockdown of *GLI2* (Figure 4C). Taken together, these findings indicate that knockdown of *GLI2* promoted cell cycle arrest in G_1 phase by inhibiting the progression of the cycle from G_1 to S phase.

Over-expression of GLI2 accelerates mesenchymal stem cell proliferation

To examine the role of GLI2 in the pathogenesis of osteosarcoma, we over-expressed GLI2. Although the origin of osteosarcoma is still controversial, it is believed that it originates from osteoblasts or mesenchymal stem cells [23]. In this regard, we studied the effects of GLI2 over-expression in the immortalized human mesenchymal stem cell line (YKNK-12) [14]. We assessed the proliferation of YKNK-12 cells following transfection with the GLI2ΔN expression vector, which exhibits potent transcriptional activity *in vivo* [24]. The MTT assay showed that forced

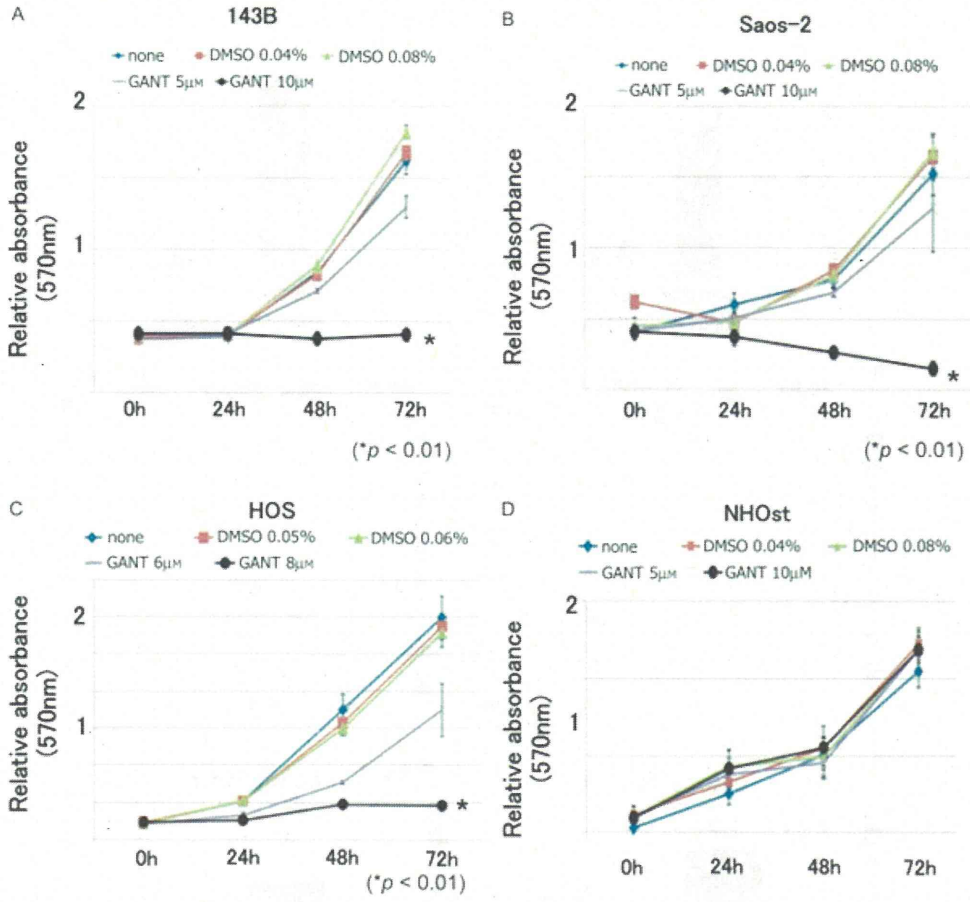

Figure 2. Inhibition of GLI prevents osteosarcoma cells proliferation. (A–C) GANT61 dose-dependently inhibited the growth of 143B, Saos-2 and HOS cells at 72 h (*$p < 0.01$). (D) At the same time point, GANT61 did not affect the growth of normal osteoblast cells (NHOst) ($n > 3$; error bars indicate SD).

expression of GLI2ΔN promoted YKNK-12 proliferation to a greater extent than transfection with control vector (Figure 5B). These findings suggest that GLI2 promotes mesenchymal stem cell proliferation. We also examined the role of GLI2 in regulating cell cycle in mesenchymal stem cells. Following forced expression of GLI2ΔN, 62.9% of the cells were in G_1 phase, 12.5% were in S phase and 22.9% were in the G_2–M phase, whereas 72.0%, 9.8% and 17.0% of cells were in G_1, S and G_2–M phases, respectively, following transfection with the control vector (Figure 5C). These findings suggest that GLI2 accelerates cell cycle progression of mesenchymal stem cells.

GLI2 knockdown inhibits osteosarcoma growth in nude mice

To confirm the role of *GLI2* knockdown in osteosarcoma growth, we tested the effects of *GLI2* knockdown in nude mice. Inoculation of 143B cells, previously transfected with *GLI2* shRNA, resulted in a statistically significant reduction of tumour growth as compared with inoculation of 143B cells transfected with control shRNA (Figure 6A). Kaplan–Meier analysis revealed that knockdown of *GLI2* in 143B cells provided a statistically significant survival benefit in mice (Figure 6B). These findings show that *GLI2* knockdown inhibits osteosarcoma cell growth in nude mice.

Discussion

Our findings demonstrate that GLI2 transcription factor significantly contributes to the growth of osteosarcoma cells. Our findings thus suggest that GLI2 might be an attractive target for therapeutic intervention, particularly in patients with high-grade and/or metastatic osteosarcoma. Small-molecule inhibitors of GLI transcription factors, such as GANT61, that efficiently inhibit the proliferation of prostate cancer cells have recently been identified [22]. MTT assay showed that GANT61 effectively inhibited osteosarcoma cell proliferation *in vitro*. We used 50 mg/kg GANT61 to inhibit GLI in a mouse xenograft model as previously described [22]. All injections were performed at a distance of 2–3 cm from the tumour site. We found no differences in osteosarcoma growth between the GANT61- and the control DMSO-treated groups (see Supporting information, Figure S1B). One possible explanation for this discrepancy is given by the difference in cell viability or permeation of GANT61

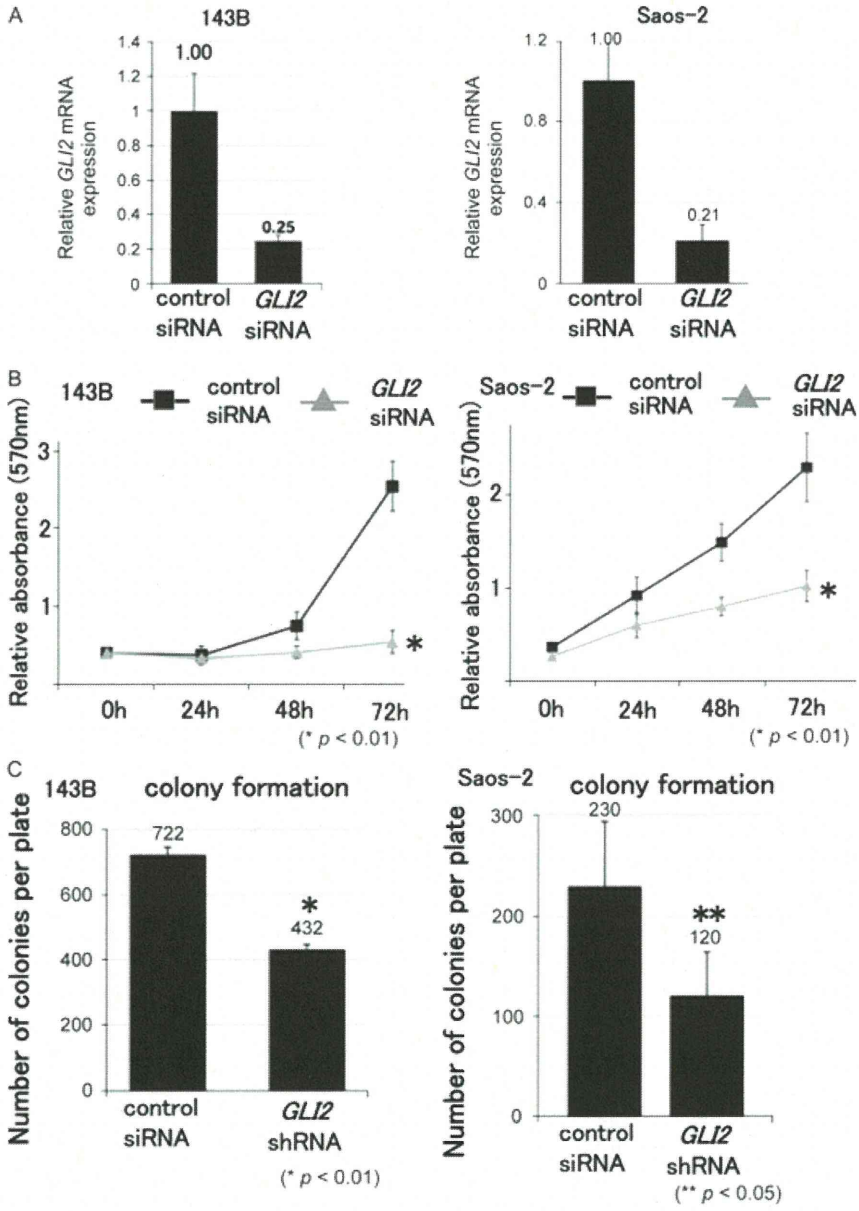

Figure 3. *GLI2* knockdown inhibits proliferation of osteosarcoma cells. (A) Transfection of *GLI2* siRNA resulted in a >70% knockdown efficiency of GLI2 [error bars represent mean (SD)]. $^{\Delta\Delta}$ Ct analysis was performed to evaluate the fold change in *GLI2* mRNA expression, using *GAPDH* or *ACTB*. (B) Growth at 72 h of 143B and Saos-2 cells was inhibited by *GLI2* siRNA. The experiment was performed in triplicate with similar results ($^{*}p < 0.01$) [error bars represent mean (SD)]. (C) A reduced number of colonies was observed in soft agar following *GLI2* knockdown. These experiments were performed in triplicate with similar results ($^{*}p < 0.01$; $^{**}p < 0.05$) [error bars represent mean (SD)].

between the osteosarcoma and prostate cancer cells *in vivo*. Nonetheless, these two studies independently suggest that low-molecular-weight compounds can inhibit malignant tumours *in vitro*. Moreover, these findings suggest that other GLI-specific inhibitors may have a powerful therapeutic potential for the management of osteosarcoma and other malignancies characterized by constitutive activation of the Hedgehog signalling pathway.

For *in vivo GLI2* RNA interference studies, we inoculated 143B osteosarcoma cells that had been previously transfected with *GLI2* shRNA. Although knockdown of *GLI2* by shRNA significantly inhibited osteosarcoma growth in nude mice, this method is not clinically applicable. Recently, the potential clinical usefulness of RNA interference in mammalian cells has been demonstrated, with no reported interferon activation [25]. In addition, Davis *et al* [26] reported a human phase I clinical trial involving the systemic administration of siRNA to patients with solid cancers; they demonstrated that siRNA administered systemically to a human can inhibit a specific gene. These findings strongly suggest that administration of *GLI2* siRNA might be a promising new treatment for osteosarcoma.

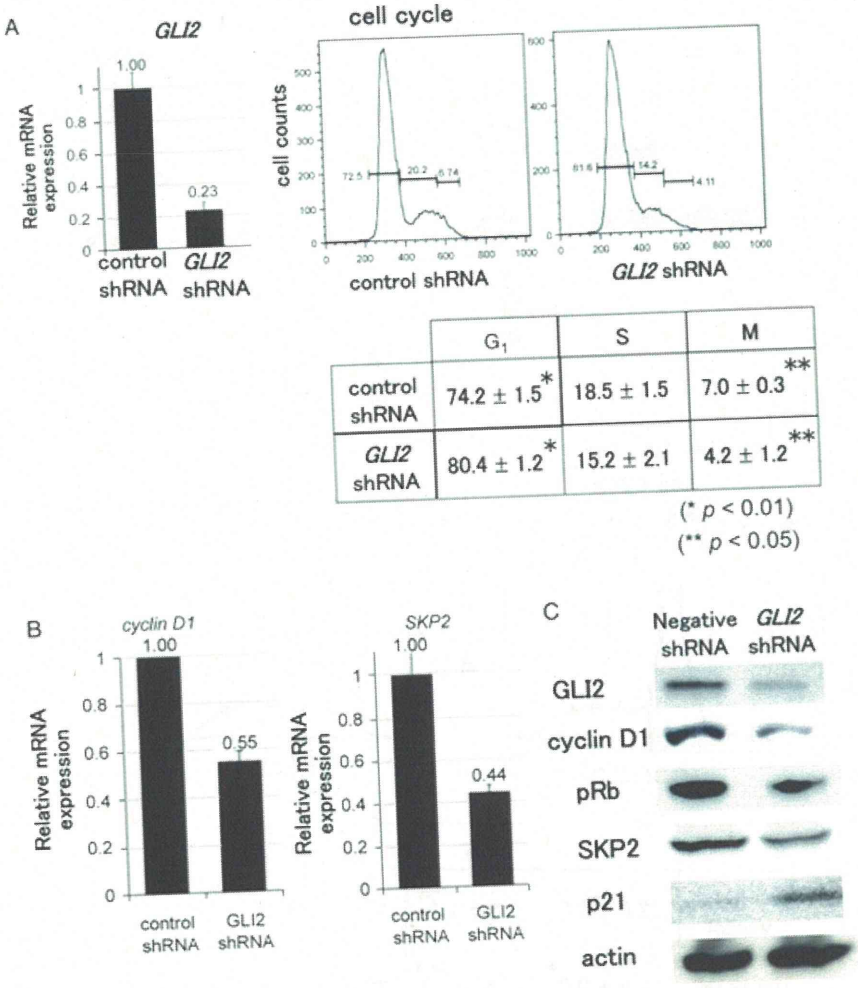

	G_1	S	M
control shRNA	74.2 ± 1.5*	18.5 ± 1.5	7.0 ± 0.3**
GLI2 shRNA	80.4 ± 1.2*	15.2 ± 2.1	4.2 ± 1.2**

(* $p < 0.01$)
(** $p < 0.05$)

Figure 4. Knockdown of *GLI2* promotes cell cycle arrest in the G_1 phase. (A) Following transfection of *GLI2* shRNA, the efficacy of *GLI2* knockdown was >75%. $^{\Delta\Delta}$ Ct analysis was performed to evaluate the fold change in mRNA expression, using *GAPDH* or *ACTB*. (B) When 143B cells were transfected with control shRNA, 74.2% of them were in G_1 phase, while when they were transfected with *GLI2* shRNA, 80.4% of the cells were in G_1 phase (* $p < 0.01$; ** $p < 0.05$). (B) Real-time PCR was employed to examine the expression of cell cycle-related genes. $^{\Delta\Delta}$ Ct analysis was performed to evaluate fold changes of mRNA expression, using *GAPDH* or *ACTB*. Knockdown of *GLI2* decreased the expression of the cell cycle accelerators, *cyclin D1* and *SKP2* [error bars represent mean (SD)]. (C) Western blot analysis revealed that knockdown of *GLI2* decreased the protein levels of cyclin D1, pRb and SKP2. Western blot analysis revealed that knockdown of *GLI2* increased the expression of *p21*^{cip1}, a negative regulator of cell cycle progression.

We previously reported that inhibition of SMO by cyclopamine or by *SMO* RNA interference reduced the growth of osteosarcoma via cell cycle regulation [21]. Compared to several potential mutational targets within the Hedgehog pathway downstream of SMO already discovered, the group of tumours that would benefit from direct GLI inhibition is substantial and likely to increase. For instance, it has been reported that inhibition of GLI, but not SMO, induced apoptosis in chronic lymphocytic leukaemia cells [27].

In order to examine the molecular mechanisms of GLI2 up-regulation, we examine genomic amplification of the GLI2 locus. We performed cytogenetic studies in three osteosarcoma specimens. FISH analysis using specific probes for the GLI2 locus revealed no chromosomal abnormalities in our osteosarcoma biopsy tissues (data not shown); this region of the genome is known to be amplified in some tumour specimens [28–32]. Further examinations should be done to elucidate the molecular mechanisms of GLI2 up-regulation.

We showed that knockdown of *GLI2* decreased the expression of SKP2 [33,34]. In addition, we found that knockdown of *GLI2* increased the expression of $p21^{Cip1}$. SKP2 is a subunit of the SCF^{SKP2} complex, a ubiquitin-dependent ligase. Down-regulation of the SCF^{SKP2} complex may promote a cell cycle arrest in G_1 phase by inhibition of $p21^{Cip1}$ degradation. Several key signalling pathways, including Hedgehog, TGFβ, BMP, Notch and Wnt, are engaged in essential processes of embryonic development. Recently, it has been clarified that these pathways also play important roles in the pathogenesis of malignant tumours (reviewed in [35]). In addition, it has been shown that there is a direct interaction or crosstalk among these key pathways (reviewed in [36]). We previously reported that

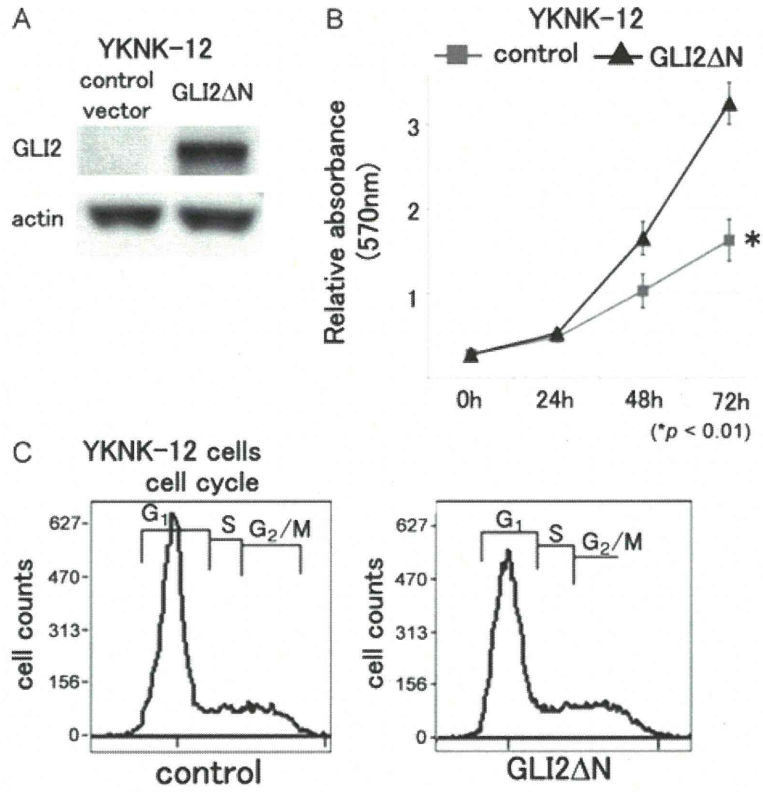

	G_1	S	M
control vector	72.0 ± 0.5*	9.8 ± 1.1**	17.0 ± 1.3*
GLI2ΔN	62.9 ± 0.9*	12.5 ± 1.0**	22.9 ± 1.5*

(*$p < 0.01$)
(**$p < 0.05$)

Figure 5. Over-expression of GLI2 accelerates mesenchymal stem cell proliferation. (A) Western blot analysis revealed that cells transfected with the GLI2ΔN expression vector reacted positively with the anti-GLI2 antibody. (B) We assessed the proliferation of YKNK-12 cells following transfection with the GLI2ΔN expression vector, which exhibits a potent transcriptional activity. The MTT assay showed that forced expression of GLI2ΔN promoted YKNK-12 cell proliferation to a greater extent than transfection with control vector (*$p < 0.01$) [error bars represent mean (SD)]. (C) Cell cycle analysis of YKNK-12 cell revealed that 62.9% and 72.0% of the cells were in G_1 phase following forced expression of GLI2ΔN and transfection with control vector, respectively. Furthermore following forced expression of GLI2ΔN, 12.5% and 22.9% of the cells were in the S and G_2–M phase, respectively, whereas 9.8% and 17.0% of the control vector-transfected cells were in the S and G_2–M phase, respectively (*$p < 0.01$; **$p < 0.05$).

the Notch pathway is activated in human osteosarcoma and that its activation promotes osteosarcoma cell growth [37]. In turn, activation of the Notch pathway promotes transcription of SKP2. SKP2 might thus mediate the crosstalk between the Notch and Hedgehog pathways. Further studies are needed to elucidate the role of interaction between these pathways in the pathogenesis of osteosarcoma.

Several recent studies have demonstrated that the anti-tumour effects of Hedgehog pathway inhibitors are mediated by their effects on tumour stromal cells [38,39]. Other studies have demonstrated that Hedgehog pathway inhibitors directly affect cancer cells [21,22,40–44]. Our findings showed that both GLI inhibition and *GLI2* knockdown directly inhibit osteosarcoma cell growth. Further studies are needed to establish the role of GLI2 activation in response to paracrine and autocrine Hedgehog signalling in osteosarcoma cells.

The hypothesis that malignant tumours are generated by rare populations of tumour-initiating cells (TICs), also called cancer stem cells, that are more tumourigenic than other cancer cells, has gained increasing credence [22,45]. We and others have reported that some bone and soft tissue sarcomas are generated by TICs [16,46]. The Hedgehog pathway has been implicated in the maintenance of normal stem cell or progenitor cells in many tissues, including the epithelia of many internal organs and brain [47]. Magali *et al* [48,49] reported that inhibition of Hedgehog

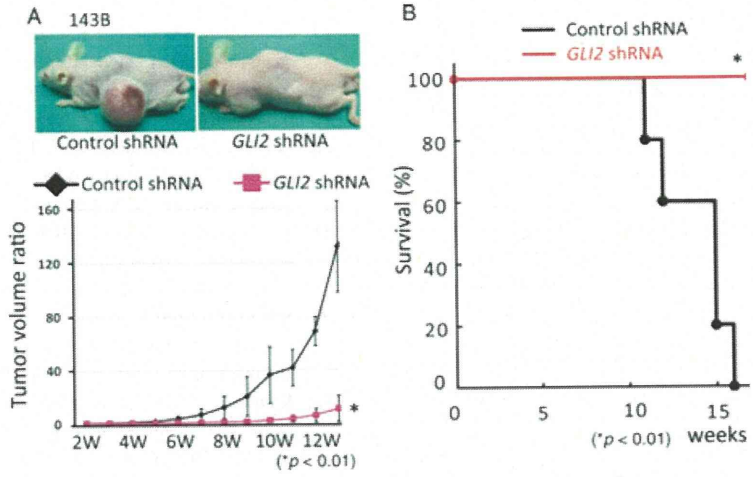

Figure 6. *GLI2* knockdown inhibits osteosarcoma growth in nude mice. (A) Following transfection of control shRNA or *GLI2* shRNA, 1×10^6 143 B cells were subcutaneously inoculated in nude mice. Tumour size was calculated weekly by using the formula $LW^2/2$ (where L and W represent the length and width of tumours). Seven days after inoculation, tumour volume was set as 1 and the increase in tumour volume was calculated at different time points, using the above formula. *GLI2* shRNA-transfected cells demonstrated a significant inhibition of tumour growth as compared with control shRNA-transfected cells ($n = 6$; $^*p < 0.01$) [error bars represent mean (SD)]. Kaplan–Meier analysis revealed that knockdown of *GLI2* provided a significant survival benefit ($n = 6$; $^*p < 0.01$).

signalling depletes TICs, whereas constitutive activation of Hedgehog signalling increases the number of TICs and accelerates tumour progression. These findings suggest that inhibition of the Hedgehog pathway might decrease the proportion of osteosarcoma TICs. The presence of a high aldehyde dehydrogenase (ALDH) activity has been used to identify TICs in malignant tumours [50–52]. Recently, Wang *et al* [53] reported that TICs obtained from osteosarcoma can be identified by a high ALDH activity. In this regard, we determined the proportion of cells with a high ALDH activity following *GLI2* siRNA transfection. At baseline, 30.6% of 143B cells showed a high ALDH activity. Seven days after *GLI2* siRNA transfection, there was no change in the proportion of cells with a high ALDH activity (data not shown). Further studies are needed to determine the impact of Hedgehog pathway inhibition on the proportion of TICs in other osteosarcoma cell lines or using other methodologies to identify TICs. In conclusion, our findings demonstrate that inhibition of GLI2 prevents osteosarcoma growth. These finding improves our understanding of osteosarcoma pathogenesis and suggest that inhibitions of GLI2 may be regarded as an effective treatment for patients with osteosarcoma.

Acknowledgment

We are grateful to Hui Gao for excellent technical assistance. We thank Dr Naoya Kobayashi (Department of Surgery, Okayama University Graduate School of Medicine and Dentistry, Japan) for providing the YKNK-12 cell line. We thank H Sasaki (Laboratory for Embryonic Induction, RIKEN Centre for Developmental Biology, Kobe, Japan) for providing the reporter vectors. This work was supported by Grants-in-Aid for Scientific Research (KAKENHI) (B) 18390419, (C) 19591725, (C) 20591786, (C) 21591919, (C) 21591920, and (C) 22591663 and a Grant-in-Aid from the Ministry of Health, Labour, and Welfare of Japan for the Third Term Comprehensive Control Research for Cancer.

Author contributions

NH, IY, NS, KS and ST conceived and designed the experiments. NH, HM, YT and TT performed the experiments. IK, NK, KS and ST analysed the data. NH and HM contributed reagents/materials/analysis tools. ST drafted the manuscript.

References

1. Sweetnam R. Osteosarcoma. *Br J Hosp Med* 1982; **28**: ,116 112–121.
2. Dorfman HD, Czerniak B. Bone cancers. *Cancer* 1995; **75**: 203–210.
3. Wu PK, Chen WM, Chen CF, *et al*. Primary osteogenic sarcoma with pulmonary metastasis: clinical results and prognostic factors in 91 patients. *Japan J Clin Oncol* 2009; **39**: 514–522.
4. Iwamoto Y, Tanaka K, Isu K, *et al*. Multi-institutional phase II study of neoadjuvant chemotherapy for osteosarcoma (NECO study) in Japan: NECO-93J and NECO-95J. *J Orthop Sci* 2009; **14**: 397–404.
5. Meyers PA, Schwartz CL, Krailo M, *et al*. Osteosarcoma: a randomized, prospective trial of the addition of ifosfamide and/or muramyl tripeptide to cisplatin, doxorubicin, and high-dose methotrexate. *J Clin Oncol* 2005; **23**: 2004–2011.
6. Kager L, Zoubek A, Kastner U, *et al*. Skip metastases in osteosarcoma: experience of the Cooperative Osteosarcoma Study Group. *J Clin Oncol* 2006; **24**: 1535–1541.
7. Horowitz JM, Park SH, Bogenmann E, *et al*. Frequent inactivation of the retinoblastoma anti-oncogene is restricted to a subset of human tumor cells. *Proc Natl Acad Sci USA* 1990; **87**: 2775–2779.

8. Ingham PW, McMahon AP. Hedgehog signaling in animal development: paradigms and principles. *Genes Dev* 2001; **15**: 3059–3087.
9. Ruiz i Altaba A, Sanchez P, Dahmane N. Gli and hedgehog in cancer: tumours, embryos and stem cells. *Nat Rev* 2002; **2**: 361–372.
10. Lum L, Beachy PA. The Hedgehog response network: sensors, switches, and routers. *Science (NY)* 2004; **304**: 1755–1759.
11. Bijlsma MF, Spek CA, Peppelenbosch MP. Hedgehog: an unusual signal transducer. *Bioessays* 2004; **26**: 387–394.
12. Ding Q, Motoyama J, Gasca S, *et al*. Diminished sonic hedgehog signaling and lack of floor plate differentiation in *Gli2* mutant mice. *Development (Camb UK)* 1998; **125**: 2533–2543.
13. Ruiz i Altaba A, Mas C, Stecca B. The *Gli* code: an information nexus regulating cell fate, stemness and cancer. *Trends Cell Biol* 2007; **17**: 438–447.
14. Nakahara H, Misawa H, Hayashi T, *et al*. Bone repair by transplantation of hTERT-immortalized human mesenchymal stem cells in mice. *Transplantation* 2009; **88**: 346–353.
15. Hijioka H, Setoguchi T, Miyawaki A, *et al*. Up-regulation of Notch pathway molecules in oral squamous cell carcinoma. *Int J Oncol* 2010; **36**: 817–822.
16. Hirotsu M, Setoguchi T, Matsunoshita Y, *et al*. Tumour formation by single fibroblast growth factor receptor 3-positive rhabdomyosarcoma-initiating cells. *Br J Cancer* 2009; **101**: 2030–2037.
17. Sasaki H, Hui C, Nakafuku M, *et al*. A binding site for Gli proteins is essential for HNF-3β floor plate enhancer activity in transgenics and can respond to Shh *in vitro*. *Development (Camb, UK)* 1997; **124**: 1313–1322.
18. Sasaki H, Nishizaki Y, Hui C, *et al*. Regulation of Gli2 and Gli3 activities by an amino-terminal repression domain: implication of Gli2 and Gli3 as primary mediators of Shh signaling. *Development (Camb, UK)* 1999; **126**: 3915–3924.
19. Fukushima M, Setoguchi T, Komiya S, *et al*. Retinal astrocyte differentiation mediated by leukemia inhibitory factor in cooperation with bone morphogenetic protein 2. *Int J Dev Neurosci* 2009; **27**: 685–690.
20. Sasaki H, Setoguchi T, Matsunoshita Y, *et al*. The knock-down of over-expressed EZH2 and BMI-1 does not prevent osteosarcoma growth. *Oncology Rep* 2010; **23**: 677–684.
21. Hirotsu M, Setoguchi T, Sasaki H, *et al*. Smoothened as a new therapeutic target for human osteosarcoma. *Mol Cancer* 2010; **9**: 5.
22. Lauth M, Bergstrom A, Shimokawa T, *et al*. Inhibition of GLI-mediated transcription and tumor cell growth by small-molecule antagonists. *Proc Natl Acad Sci USA* 2007; **104**: 8455–8460.
23. Tang N, Song WX, Luo J, *et al*. Osteosarcoma development and stem cell differentiation. *Clin Orthop Rel Res* 2008; **466**: 2114–2130.
24. Roessler E, Ermilov AN, Grange DK, *et al*. A previously unidentified amino-terminal domain regulates transcriptional activity of wild-type and disease-associated human *GLI2*. *Hum Mol Genet* 2005; **14**: 2181–2188.
25. Elbashir SM, Harborth J, Lendeckel W, *et al*. Duplexes of 21-nucleotide RNAs mediate RNA interference in cultured mammalian cells. *Nature* 2001; **411**: 494–498.
26. Davis ME, Zuckerman JE, Choi CH, *et al*. Evidence of RNAi in humans from systemically administered siRNA via targeted nanoparticles. *Nature* 2010; **464**: 1067–1070.
27. Desch P, Asslaber D, Kern D, *et al*. Inhibition of GLI, but not Smoothened, induces apoptosis in chronic lymphocytic leukemia cells. *Oncogene* 2010; **29**: 4885–4895.
28. Gimenez S, Costa C, Espinet B, *et al*. Comparative genomic hybridization analysis of cutaneous large B-cell lymphomas. *Exp Dermatol* 2005; **14**: 883–890.
29. Fishman A, Shalom-Paz E, Fejgin M, *et al*. Comparing the genetic changes detected in the primary and secondary tumor sites of ovarian cancer using comparative genomic hybridization. *Int J Gynecol Cancer* 2005; **15**: 261–266.
30. Liu XP, Sato T, Oga A, *et al*. Two subtypes of mucinous colorectal carcinoma characterized by laser scanning cytometry and comparative genomic hybridization. *Int J Oncol* 2004; **25**: 615–621.
31. Wreesmann VB, Ghossein RA, Hezel M, *et al*. Follicular variant of papillary thyroid carcinoma: genome-wide appraisal of a controversial entity. *Genes Chromosomes Cancer* 2004; **40**: 355–364.
32. Wei G, Lonardo F, Ueda T, *et al*. *CDK4* gene amplification in osteosarcoma: reciprocal relationship with *INK4A* gene alterations and mapping of 12q13 amplicons. *Int J Cancer* 1999; **80**: 199–204.
33. Kamura T, Hara T, Matsumoto M, *et al*. Cytoplasmic ubiquitin ligase KPC regulates proteolysis of p27(Kip1) at G_1 phase. *Nat Cell Biol* 2004; **6**: 1229–1235.
34. Hara T, Kamura T, Kotoshiba S, *et al*. Role of the UBL-UBA protein KPC2 in degradation of p27 at G_1 phase of the cell cycle. *Mol Cell Biol* 2005; **25**: 9292–9303.
35. Rubin LL, de Sauvage FJ. Targeting the Hedgehog pathway in cancer. *Nat Rev Drug Discov* 2006; **5**: 1026–1033.
36. Ross J, Li L. Recent advances in understanding extrinsic control of hematopoietic stem cell fate. *Curr Opin Hematol* 2006; **13**: 237–242.
37. Tanaka M, Setoguchi T, Hirotsu M, *et al*. Inhibition of Notch pathway prevents osteosarcoma growth by cell cycle regulation. *Br J Cancer* 2009; **100**: 1957–1965.
38. Tian H, Callahan CA, DuPree KJ, *et al*. Hedgehog signaling is restricted to the stromal compartment during pancreatic carcinogenesis. *Proc Natl Acad Sci USA* 2009; **106**: 4254–4259.
39. Yauch RL, Gould SE, Scales SJ, *et al*. A paracrine requirement for hedgehog signalling in cancer. *Nature* 2008; **455**: 406–410.
40. Sanchez P, Hernandez AM, Stecca B, *et al*. Inhibition of prostate cancer proliferation by interference with sonic hedgehog–GLI1 signaling. *Proc Natl Acad Sci USA* 2004; **101**: 12561–12566.
41. Singh RR, Cho-Vega JH, Davuluri Y, *et al*. Sonic hedgehog signaling pathway is activated in ALK-positive anaplastic large cell lymphoma. *Cancer Res* 2009; **69**: 2550–2558.
42. Lindemann RK. Stroma-initiated hedgehog signaling takes center stage in B-cell lymphoma. *Cancer Res* 2008; **68**: 961–964.
43. Wong SY, Seol AD, So PL, *et al*. Primary cilia can both mediate and suppress Hedgehog pathway-dependent tumorigenesis. *Nat Med* 2009; **15**: 1055–1061.
44. Dierks C, Beigi R, Guo GR, *et al*. Expansion of *Bcr-Abl*-positive leukemic stem cells is dependent on Hedgehog pathway activation. *Cancer Cell* 2008; **14**: 238–249.
45. Clarke MF, Fuller M. Stem cells and cancer: two faces of Eve. *Cell* 2006; **124**: 1111–1115.
46. Murase M, Kano M, Tsukahara T, *et al*. Side population cells have the characteristics of cancer stem-like cells/cancer-initiating cells in bone sarcomas. *Br J Cancer* 2009; **101**: 1425–1432.
47. Beachy PA, Karhadkar SS, Berman DM. Tissue repair and stem cell renewal in carcinogenesis. *Nature* 2004; **432**: 324–331.
48. Dierks C, Grbic J, Zirlik K, *et al*. Essential role of stromally induced hedgehog signaling in B-cell malignancies. *Nat Med* 2007; **13**: 944–951.
49. Zhao C, Chen A, Jamieson CH, *et al*. Hedgehog signalling is essential for maintenance of cancer stem cells in myeloid leukaemia. *Nature* 2009; **458**: 776–779.
50. Ginestier C, Hur MH, Charafe-Jauffret E, *et al*. ALDH1 is a marker of normal and malignant human mammary stem cells and a predictor of poor clinical outcome. *Cell Stem Cell* 2007; **1**: 555–567.

51. Huang EH, Hynes MJ, Zhang T, *et al*. Aldehyde dehydrogenase 1 is a marker for normal and malignant human colonic stem cells (SC) and tracks SC overpopulation during colon tumorigenesis. *Cancer Res* 2009; **69**: 3382–3389.
52. Cheung AM, Wan TS, Leung JC, *et al*. Aldehyde dehydrogenase activity in leukemic blasts defines a subgroup of acute myeloid leukemia with adverse prognosis and superior NOD/SCID engrafting potential. *Leukemia* 2007; **21**: 1423–1430.
53. Wang L, Park P, Zhang H, *et al*. Prospective identification of tumorigenic osteosarcoma cancer stem cells in OS99–1 cells based on high aldehyde dehydrogenase activity. *Int J Cancer* 2011; **128**: 294–303.

SUPPORTING INFORMATION ON THE INTERNET

The following supporting information may be found in the online version of this article:

Figure S1. Knockdown of GLI2 promotes cell arrest of Saos-2 cell.

EMBO
Molecular Medicine

Insulin biosynthesis in neuronal progenitors derived from adult hippocampus and the olfactory bulb

Tomoko Kuwabara[1], Mohamedi N. Kagalwala[2], Yasuko Onuma[1], Yuzuru Ito[1], Masaki Warashina[1†], Kazuyuki Terashima[1], Tsukasa Sanosaka[3], Kinichi Nakashima[3], Fred H. Gage[2], Makoto Asashima[1]***

Keywords: diabetes; hippocampus; insulin; neural stem cell; olfactory bulb

DOI 10.1002/emmm.201100177

Received March 08, 2011
Revised August 04, 2011
Accepted August 08, 2011

→See accompanying article
http://dx.doi.org/10.1002/emmm.201100178

In the present study, we demonstrated that insulin is produced not only in the mammalian pancreas but also in adult neuronal cells derived from the hippocampus and olfactory bulb (OB). Paracrine Wnt3 plays an essential role in promoting the active expression of insulin in both hippocampal and OB-derived neural stem cells. Our analysis indicated that the balance between Wnt3, which triggers the expression of insulin via NeuroD1, and IGFBP-4, which inhibits the original Wnt3 action, is regulated depending on diabetic (DB) status. We also show that adult neural progenitors derived from DB animals retain the ability to give rise to insulin-producing cells and that grafting neuronal progenitors into the pancreas of DB animals reduces glucose levels. This study provides an example of a simple and direct use of adult stem cells from one organ to another, without introducing additional inductive genes.

INTRODUCTION

There are considerable similarities between the genes expressed in the developing brain and pancreas in mammals (Edlund, 2002; Habener et al, 2005; Hori et al, 2005). In *Drosophila*, insulin is produced by neurons within the brain (Brogiolo et al, 2001; Rulifson et al, 2002). Clusters of these insulin-producing cells in flies and vertebrate pancreatic islet β cells were considered functional analogues and evolved from a common ancestral insulin-producing neuron (Rulifson et al, 2002). Insulin signalling plays important roles in the proliferation and differentiation of cells in both developmental and adult stages (Hsieh et al, 2004; McMorris and Dubois-Delcq, 1986). Insulin, IGF-1 and IGF-2 provide instructive signals for regulating cell fate choice of adult neural stem cells (NSCs) in the hippocampus (HPC) (Hsieh et al, 2004). Interestingly, diabetes impairs hippocampal learning and memory in diabetic (DB) rats and mice, thus indicating its detrimental effects on neurogenesis and synaptic neuronal plasticity (Stranahan et al, 2008). Moreover, diabetes increases the risk of clinical depression and dementia (Greenwood and Winocur, 2005; Messier 2005).

Mammalian neurogenesis occurs throughout adulthood in the subventricular zone (SVZ) of the forebrain lateral ventricles and the HPC. In the SVZ, NSCs migrate within the rostral extension of the SVZ along the rostral migratory stream, eventually reaching the olfactory bulb (OB). Multipotent NSCs can be isolated from the easily accessible OB (Bédard and Parent, 2004; Gritti et al, 2002; Hayakawa et al, 2007; Pagano et al, 2000). Extensive studies on adult hippocampal neurogenesis have revealed that it can be modulated by physiological and behavioural events, such as aging, stress, disease, seizures and learning. In the HPC, new neurons are continuously generated from self-renewing NSCs in the dentate gyrus (DG) (D'Amour and Gage, 2003; Gage, 2000; Suh et al, 2007), a process promoted by Wnt3 released from underlying astrocytes (Lie et al, 2005). Therefore, local inhibition of Wnt signalling in the DG reduces the number of newborn neurons (Jessberger et al, 2009; Kuwabara et al, 2009; Lie et al, 2005).

(1) Research Center for Stem Cell Engineering, National Institute of Advanced Industrial Science and Technology (AIST), Tsukuba Science City, Japan
(2) Laboratory of Genetics, The Salk Institute, La Jolla, CA, USA
(3) Laboratory of Molecular Neuroscience, Graduate School of Biological Sciences, Nara Institute of Science and Technology, Takayama, Ikoma, Japan
***Corresponding author:** Tel: +81-298-61-2534; Fax: +81-298-61-2987; E-mail: t.warashina@aist.go.jp
****Corresponding author:** Tel: +81-298-61-2529; Fax:+81-298-61-2987; E-mail: m-asashima@aist.go.jp
† Present address: Genome Research Laboratories, Wako Pure Chemical Industries, Ltd., Amagasaki, Hyogo, Japan

We demonstrated that adult hippocampal Wnt/β-catenin signalling triggers NeuroD1 expression (Kuwabara et al, 2009). NeuroD1, a basic helix-loop-helix (bHLH) transcription factor, has been shown to play an important role in both developing pancreas and brain (Liu et al, 2000; Miyata et al, 1999; Naya et al, 1997, 1995). NeuroD1-deficiency in mice causes severe diabetes and perinatal lethality because NeuroD1 is required for insulin gene expression (Naya et al, 1997, 1995). Similar to the loss of Wnt/β-catenin signalling (Lee et al, 2000), NeuroD1 deficiency during hippocampal development leads to a complete loss of DG formation in mice (Liu et al, 2000; Miyata et al, 1999). Despite their separate developmental origins, the gene expression programs for developing neurons and β cells are remarkably similar (Edlund, 2002; Habener et al, 2005). However, insulin expression in the adult brain and the underlying regulatory mechanism, have not been demonstrated.

Here, we provide evidence that adult granule neurons natively express insulin. This insulin expression during neuronal differentiation was observed not only in hippocampal NSCs (HPC NSCs) but also in adult NSCs isolated from the OB (OB NSCs). Wnt3 played an important role in up-regulating endogenous NeuroD1 expression, which in turn activated insulin gene expression by the direct association of NeuroD1 with the insulin promoter in both HPC and OB NSCs. Although the contribution of Wnt3 to insulin expression was apparent, inhibitory mechanisms also played a role. Insulin-like growth factor-binding proteins (IGFBPs), which acted as inhibitory factors of Wnt-mediated promotion, were up-regulated upon neuronal differentiation. In DB animals, IGFBP-4 expression was further up-regulated, whereas, Wnt3 and NeuroD1 expression declined. Importantly, adult HPC and OB NSCs derived from DB animals retained the ability to generate insulin-producing cells. *Ex vivo* culture with Wnt3a ligand and a neutralizing antibody against IGFBP-4 significantly promoted insulin production, and grafted adult HPC and OB NSCs from DB animals became efficient sources of *de novo* insulin biosynthesis *in vivo*. Our results confirm the strong functional similarity between adult neurons and β cells and suggest possible approaches to cell replacement therapy for diabetes.

RESULTS

Hippocampal neurons express insulin and C-peptide

We first investigated *insulin-1* mRNA expression in adult HPC by *in situ* hybridization. Positive *insulin-1* mRNA signals were detected at granule cell layers (GCL) in DG (Fig 1A; negative controls are shown in Fig S1A of Supporting information). Strong signals were observed in neuronal layers but were not found in cells at the inner layer of the DG where astrocytes and undifferentiated NSCs reside. Signals were also detected in CA1 and CA3 pyramidal neuron layers (Fig S1B of Supporting information).

The expression of insulin-1 protein in adult HPC and pancreas was examined in parallel by enzyme-linked immunosorbent assay (sandwich enzyme-linked immunosorbent assay; ELISA). Although the insulin expression level was significantly higher in the pancreas than in the brain (>10-fold), adult brain and HPC contained released insulin (Fig S2 of Supporting information). Insulin expression was also analysed immunohistochemically (IHC). Insulin-producing cells were clearly detected in granule neurons in DG, and these cells expressed β-tubulin III (TUJ1, Fig 1B). Insulin was expressed in the cell body and extensively in neurites extending from neurons (Fig 1B; molecular layer). Neurons in the CA1 pyramidal region, cortex and substantia nigra were also positive (Fig S3 of Supporting information). Adult pancreatic islet β cells were TUJ1+ (Fig S3B of Supporting information), suggesting similar gene expression between β cells and neurons. In DG neurons, *de novo* insulin production was confirmed by the simultaneous detection of C-peptide (Fig 1C), similar to that in pancreatic islets (Fig S3C of Supporting information). From these *in situ* hybridization, ELISA and IHC data, we confirmed that adult hippocampal neurons endogenously expressed insulin to a lesser extent than pancreatic islets.

Pancreatic α cells release Wnt3, and its level is decreased in diabetic rats

Because neurons produced insulin (Fig 1), we were interested in the niches that supported neuronal differentiation. Astrocytes define the HPC niche (Song et al, 2002), and astrocyte-secreting Wnt3 factors (Fig S4A of Supporting information) have instructive effects in promoting adult neurogenesis (Lie et al, 2005). Glial fibrillary acidic protein (GFAP) is an astrocyte marker, and GFAP-expressing (GFAP+) cells were detected in pancreatic α cells (Fig S4B of Supporting information). Interestingly, IHC revealed that the pancreatic GFAP+ cells co-localized with Wnt3+ cells (Fig 2A), indicating that α cells release the neurogenic Wnt3 as do hippocampal astrocytes.

In diabetes, deficits in insulin secretion influence the pancreatic endocrine system and HPC function (Stranahan et al, 2008). To determine Wnt3 expression under physiological changes, we compared the Wnt3+ cell population between wild-type and DB rats. In both streptozotocin (STZ)-induced type 1 DB and type II DB Goto-Kakizaki (GK) rats, marked reductions in Wnt3+ cells were observed in the pancreas Fig 2B, left; $p < 0.001$, data represent +s.d. $n = 6$ *per* group), which was also observed in the HPCs of DB rats (Fig 2B, right). Following the reduction in Wnt3+ cells in DB rats, the expression of *Wnt3* mRNA was down-regulated consistently in both pancreatic islets and the HPC (Fig 2C and D). Insulin, IGF-1 and IGF-2 were also down-regulated. Interestingly, IGFBP-4 expression was up-regulated in DB rats (Fig 2C and D).

A family of IGF-binding proteins (Firth and Baxter, 2002) modulates the bioactivity of IGF and impairs Wnt/β-catenin signalling (Zhu et al, 2008). The most potent canonical Wnt inhibitor in the IGFBP family is IGFBP-4 (Zhu et al, 2008). In diabetes, potent competitors (IGF-1 and IGF-2) of IGFBP-4 were down-regulated and the Wnt3 inhibitor IGFBP-4 was present in higher levels; further, the HPC and pancreas expressed lower levels of Wnt3.

Adult neural progenitor cells from the HPC and OB

Manipulating endogenous NSCs or transplanting the progeny of exogenously expanded neural progenitors may lead to

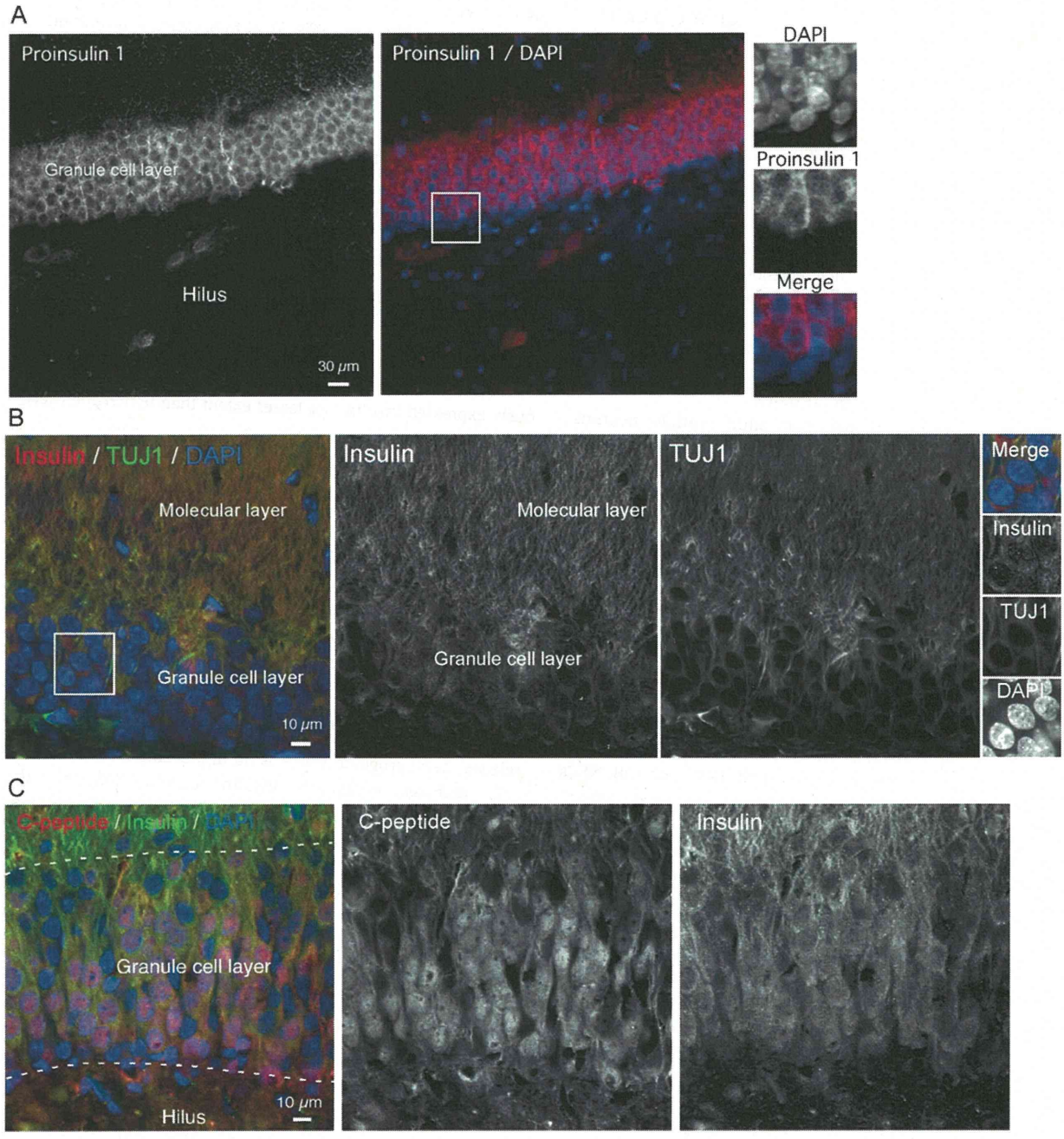

Figure 1. Adult hippocampal neurons express insulin.

A. *In situ* hybridization of proinsulin 1 mRNA in adult rat HPC. *In situ* hybridization of insulin and DAPI staining in the DG region are shown. Cells in the white square region are magnified and shown in separate panels at right. Proinsulin 1, red; DAPI, blue.

B. Immunohistochemistry analysis of insulin in DG of adult HPC. Insulin-immunoreactive cells (red) were detected in both the GCL and molecular layer of HPC, and they also expressed β tubulin III (TUJ1, green). Cells in the white square region are magnified and shown in separate panels at right. Insulin, red; TUJ1, green; DAPI, blue.

C. Detection of C-peptide in adult granule neurons in DG of HPC. C-peptide is generated when proinsulin is split into insulin and C-peptide. C-peptide, red; Insulin, green; DAPI, blue.

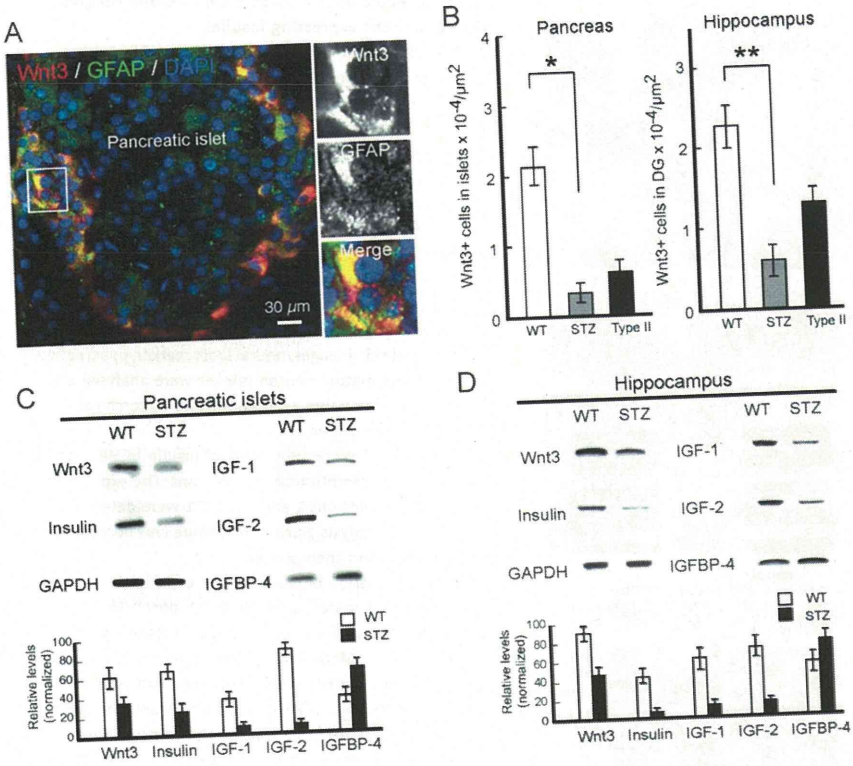

Figure 2. Wnt3, released from pancreatic α cells, decreases in diabetes.

A. Detection of Wnt3 in the pancreatic α cells expressing GFAP. A confocal image of IHC of Wnt3 and GFAP in adult pancreatic islet is shown. Cells in the white square region are magnified and shown in separate panels at right. Wnt3, red; GFAP, green; DAPI, blue.

B. Comparison of the number of Wnt3-positive cells in pancreas (left) and in DG of HPC (right) obtained from wild-type and diabetes rats. White bars, wild-type Fisher 344 rats (10-week old, male); grey bars, STZ-induced type I DB rats (10-week old, male); type II DB GK rats (10-week old, male). $^{*}p < 0.01$ and $^{**}p < 0.001$.

C. Comparison of mRNA levels of Wnt3, insulin, IGFs and IGFBP-4 between wild-type and DB animals (STZ-induced DB rats) in the pancreas.

D. Comparison of mRNA levels of Wnt3, insulin, IGFs and IGFBP-4 between wild-type and DB animals (STZ-induced DB rats) in the HPC. Relative levels of mRNA were normalized to GAPDH in the following Q-PCR analysis and are plotted at bottom.

successful cell replacement therapies for various diseases. The discovery of insulin expression in neurons prompted us to use adult NSCs without exogenous gene induction as sources of insulin-producing cells from the patient's own organs to treat diabetes. HPC NSCs are well established and have been studied extensively, whereas, OB NSCs are of potential interest because of their easily accessible location (Curtis et al, 2007; Liu and Martin, 2003; Pagano et al, 2000; Zhang et al, 2004).

HPC NSCs were round and retained this shape when expanded as a monolayer (Fig 3A, left). OB NSCs grew as heterogeneous forms with adherent property and neurosphere morphologies (Fig 3A, right). Under neuron differentiation conditions, the cell morphologies changed markedly: both HPC and OB NSCs extended prolonged neurites (Fig 3B). Gene expression profiles were measured using Agilent rat genome microarrays (Table 1 of Supporting information). HPC NSC, OB NSC and HPC and OB neuron expression profiles were grouped by hierarchical clustering, and correlation coefficients were computed for all pair-wise comparisons (Fig S5 of Supporting information). Both HPC NSCs and OB NSCs expressed the NSC marker *Sox2*, the radial glial cell marker *nestin* and the neural progenitor markers *Olig2* and *Sox1* (NSC lineage; Fig 3C). NSC marker gene expression was down-regulated in HPC and OB neurons (HPC Neu and OB Neu in Fig 3C), and neuronal marker gene expression was up-regulated (mature neuron marker; Fig 3C), indicating their successful commitment into neuronal lineages.

Importantly, *insulin-1* and *insulin-2* expression increased extensively in HPC and OB neurons (pancreatic genes; Fig 3C). IHC revealed that rat OB neurons were insulin+ natively (Fig S3D of Supporting information), consistent with the microarray data. *Pax3*, an early developmental stage neural crest marker was not detectable. Another neural crest marker, *Sox10*, was expressed in these cells, but the levels were unchanged upon neuronal differentiation. These data suggested that insulin was up-regulated in neurons derived from adult NSCs in both the HPC and OB and that its regulation in adult neuronal lineages could be distinguished from the commitment event in embryonic neural crest lineages.

In the pancreatic lineage, insulin gene expression is regulated by several transcription factors abundant in islets such as NeuroD1, neurogenin 3 Pdx1 and MafA (Melloul et al, 2002; Sander and German, 1997; Servitja and Ferrer, 2004). MafA and MafB are co-expressed in insulin+ β cells during embryogenesis, whereas, in the adult pancreas, only MafA is produced in β cells and MafB in glucagon+ α cells (Nishimura et al, 2006). Our microarray analysis revealed that neither HPC nor OB neurons expressed MafA, Pdx1 or neurogenin 3, which are necessary to activate the insulin gene in pancreatic β cell lineages. Quantitative real-time RT-PCR analysis confirmed that *insulin-1* mRNA induction was correlated with *NeuroD1* mRNA up-regulation in both the HPC and OB (Fig 3D). The *insulin-1* mRNA induction resulting from NeuroD1 siRNA transfection led to its down-regulation in neurons, whereas, *MafA*, *Pdx1* or *neurogenin 3* siRNAs had no influence (Fig 3E). These data suggested that *NeuroD1* expression is required for insulin expression in adult NSCs *in vitro*.

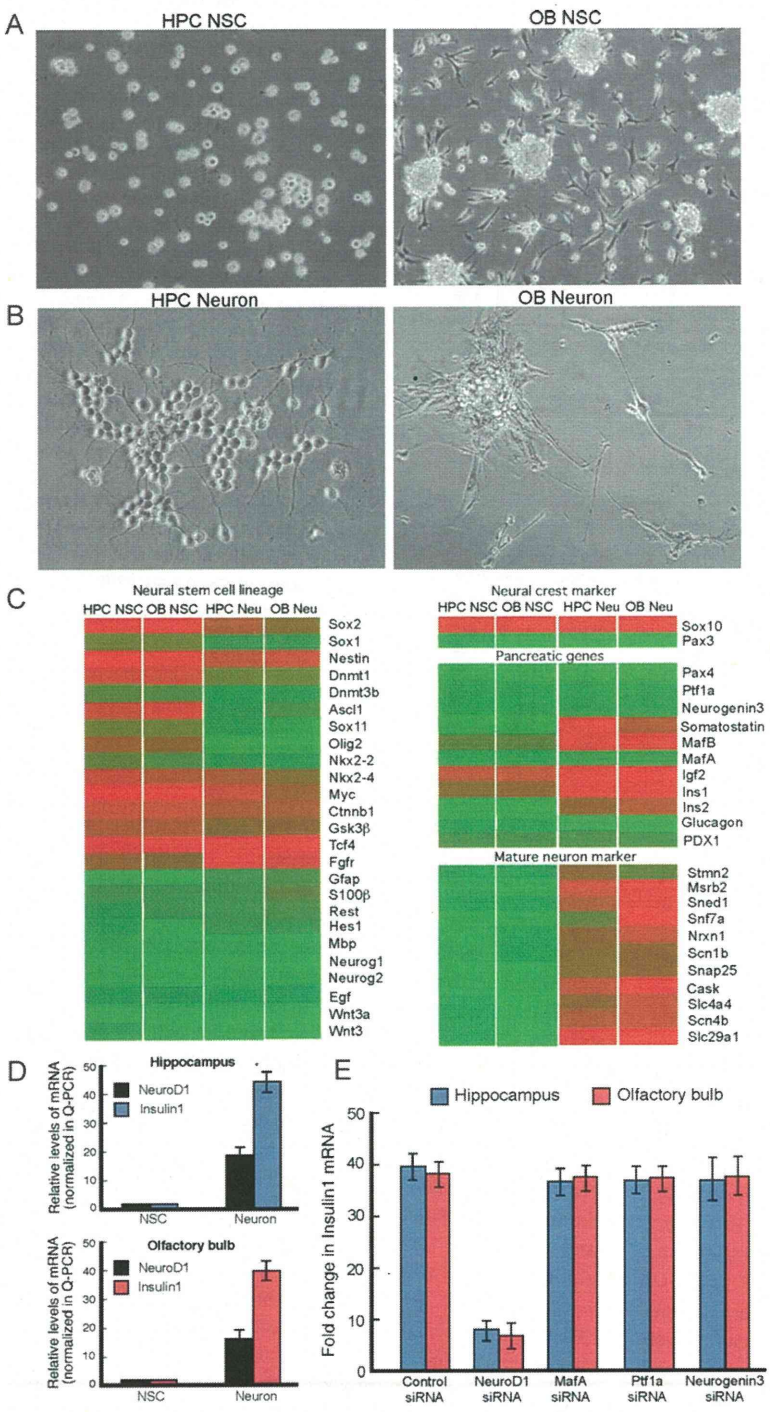

Figure 3. Adult NSCs derived from HPC and OB give rise to neurons expressing insulin.

A. The adult NSCs isolated from HPC and OB. Culture image of the proliferating hippocampal NSCs (HPC NSC, left) and NSCs derived from OB (OB NSC, right) of 7- to 8-week-old female Fisher 344 rats.

B. *In vitro* differentiated adult HPC- and OB neurons. When the culture was exposed to neuron differentiation conditions (RA + FSK + KCl), both HPC and OB cells extended neuritis (HPC neuron, left; OB neuron, right).

C. Gene expression profiles of HPC NSC, OB NSC, HPC neuron and OB neuron that were measured using Agilent rat genome microarrays. Typical genes for neuronal cell lineages, neural crest marker, pancreatic genes and mature neuron marker were analysed and the heat map using average-linkage hierarchical clustering is shown.

D. Induction of expression levels of insulin in HPC- and OB NSCs differentiating into neurons. The expression levels of proinsulin 1 and NeuroD1 were determined by Q-PCR analysis. Each mRNA value was normalized to GAPDH and then plotted.

E. Down-regulation of the neuronal expression of proinsulin 1 mRNAs with NeuroD1 siRNA. The neuronal induction of proinsulin 1 mRNA using siRNAs for NeuroD1, MafA, Pdx1 or Neurogenin 3 in HPC and OB neurons was examined in qRT-PCR analysis. Contol siRNA (scrambled siRNA) was transfected similarly. For quantification, the level of the control siRNA in NSCs group was set at 1, and the experimental siRNAs in neurons were then normalized accordingly.

Regulation of insulin expression in OB and HPC neurons

Neuronal insulin expression required NeuroD1 but not MafA, Pdx1 or neurogenin 3 (Fig 3). For NeuroD1 induction, paracrine Wnt3 plays an essential role in HPC. We determined that OB NSCs and HPC NSCs responded similarly and in a dose-dependent manner to Wnt3a ligands (Fig S6A of Supporting information). Moreover, the Wnt antagonist Dickkopf1 (Dkk1) down-regulated the expression of the TCF/LEF reporter (Fig S6A of Supporting information). These data suggested that canonical Wnt signalling is regulated analogously in both adult HPC and OB NSCs *in vitro*.

We detected IGF-binding proteins in the comparative profile analysis of adult NSCs and neurons (Fig S5 of Supporting information and Tables 1–5 of Supporting information). Thus,

IGFBP-2, IGFBP-3, IGFBP-4, IGFBP-5 and IGFBP-7 were expressed at high levels in both HPC and OB neurons (Fig S6B of Supporting information). The up-regulation of TCF/LEF reporter activity by the Wnt3a ligand was significantly inhibited by IGFBP-4 (Fig S6C of Supporting information). Treatment with an IGFBP-4 (anti-IGFBP-4)-neutralizing antibody attenuated the IGFBP-4-dependent reduction of TCF/LEF-reporter expression (Fig S6C of Supporting information). We did not detect clear effects of IGF-2, suggesting a specific inhibitory effect of IGFBP-4 on Wnt signalling.

Wnt3a treatment induced activation of the NeuroD1 promoter (Fig S6D of Supporting information). The reporter assay revealed the negative action of IGFBP-4 against Wnt3a on the *NeuroD1* promoter (Fig S6D of Supporting information). The activation of the *insulin-1* promoter by Wnt3a and anti-IGFBP activity was confirmed in both adult OB and HPC NSCs (Fig S6E of Supporting information). Chromatin immunoprecipitation (ChIP) analysis indicated that Sox2, HDAC1, dimethylation of histone H3 lysine 9 (Met-K9) and heterochromatin protein-1 (HP1) were associated on the endogenous *NeuroD1* promoter, suggesting a repressive chromatin state in NSCs (control, Fig S6F of Supporting information). In contrast, acetylated histone H3 (Ac-H3) was detected bound to the NeuroD1 promoter locus upon the introduction of Wnt3a and anti-IGFBP-4 (Fig S6F of Supporting information). The treatment led to associations of β-catenin, TCF4, dimethylation of histone H3 lysine 4 (Met-K4) and CREB-binding protein (CBP), indicating active NeuroD1 mRNA expression (Fig S6F of Supporting information). Similar complexes were detected in studies on chromatin remodelling of the E-box sequence region (Naya et al, 1997) on the insulin promoter (Fig S6G of Supporting information). Furthermore, the association of NeuroD1 with the *insulin* promoter was detected (Fig S6G of Supporting information). These data indicate that Wnt signalling promoted *insulin-1* expression via NeuroD1 activation in HPC and OB NSCs.

Wnt/β-catenin-signalling adult NSCs are required to generate pancreatic insulin-producing cells

Although neurons prepared *in vitro* and the native HPC and OB neurons expressed insulin, questions remained about whether adult NSCs can survive and potentially produce insulin within the pancreas. Although Wnt3 was produced in pancreatic α cells (Fig 2A), it is unknown whether adult NSCs respond to the Wnt3 in the pancreas. We, therefore, transplanted adult NSCs into the pancreas. We employed the Rosa-GFP mouse line to trace the fate of transplanted cells, which were transduced with $Sox2^{Cre}$GFP (retrovirus-encoding Sox2 promoter-driven Cre/GFP; Fig S7A of Supporting information). Furthermore, to examine Wnt signalling, we prepared adult HPC NSCs from β-catenin-conditional 'floxed' mice (Fig S7A of Supporting information). A retrovirus encoding $Sox2^{Cre}$GFP was infected to trace the fate of Sox2+ adult NSCs.

Adult NSCs were microinjected into adult mouse pancreas. Three weeks later, mice were injected with BrdU daily for 10 days. In the control (Control NSC TP), $Sox2^{Cre}$GFP+ cells co-localized with insulin (Fig 4A), C-peptide (Fig S7B of Supporting information) and NeuroD1 (Fig S7C of Supporting information). Interestingly, we found that $Sox2^{Cre}$GFP+ cells expressed MafA (Fig 4C) and pancreas transcription factor 1a (Ptf1a; Fig 4D). In microarray analysis (Fig 3C), adult NSCs did not express pancreatic β cells markers such as *MafA*. During embryonic development, lineage commitment of endocrine progenitors requires PTF1a (Kawaguchi et al, 2002). NSCs grafted in the pancreas, expressed β cell-specific markers such as PTF1a and MafA, suggesting that adult NSCs possessed the intrinsic ability to express these β cell-specific markers and that their expression levels were modulated by extracellular factors.

In β-catenin cKO NSC transplants (β-catenin cKO NSC TP), GFP+ cells decreased compared to that in control NSC TP mice (Fig 4F). Although $Sox2^{Cre}$GFP+ cells were detected, they did not express insulin (Fig 4B). Marker-positive cells with NeuroD1, PTF1a and MafA were rare in β-catenin cKO NSC TP mice (Fig 4G and Fig S7E of Supporting information). Sixty percent of $Sox2^{Cre}$GFP+ cells became insulin+ and C-peptide+ (control, Fig 4H). The proportion of (BrdU+ GFP+)/total GFP+ cells was higher in controls than in β-catenin cKO NSC TP mice (Fig 4I). Furthermore, the proportion of (insulin+ GFP+)/total GFP+ cells in β-catenin cKO NSC TP mice was 86% less than that in controls (Fig 4G). Some downstream β-catenin cKO NSC cell lineages were nestin+ (Fig 4E) and GFAP+ (Fig S7D of Supporting information). Since nestin is a neural progenitor marker (e.g. radial stem-like cells) and astrocytes specifically express GFAP, we hypothesized that grafted adult NSCs lacking the ability to respond to Wnt signalling remained in an undifferentiated state or possibly underwent glial differentiation.

Because GFP+ and BrdU+ GFP+ cell numbers in β-catenin cKO NSC TP mice were decreased (Fig 4F and H), we evaluated the presence of dead/dying cells by determining caspase 3 (AC3) expression by IHC. Apoptotic AC3+ cells were more abundant in β-catenin cKO NSC TP mice (Fig 4J and Fig S7F of Supporting information), indicating that Wnt/β-catenin signalling in Sox2+ NSCs was important for their survival. These data demonstrated that transplanted adult NSCs generated insulin-producing cells in the pancreas and that Wnt/β-catenin signalling played a critical role in the cell survival and function of *de novo* insulin biosynthesis in adult NSCs microinjected into the pancreas.

Diabetes therapy by transplanting adult NSCs

Next, we examined the potency of NSCs for treating diabetes *in vivo*. In the Control TP experiment (Fig 4J), AC3 was detected in microinjected adult HPC NSCs. Therefore, a collagen sheet was prepared to avoid needle wounds within the digestive pancreas. Adult NSCs were successfully maintained on the collagen sheet (Fig S8A of Supporting information), and we detected insulin expression in neuronal progenitors (NPs, cells committed to the neuronal lineage by 24 h culture under neuron differentiation conditions, Fig S8B of Supporting information). To analyse whether glucose regulated insulin secretion (i.e. C-peptide release), we treated cells with low or high glucose concentrations (2.5 or 27.5 mM, respectively). Intracellular C-peptide levels were detectably increased in both HPC and OB NSCs (Fig S8C of Supporting information).

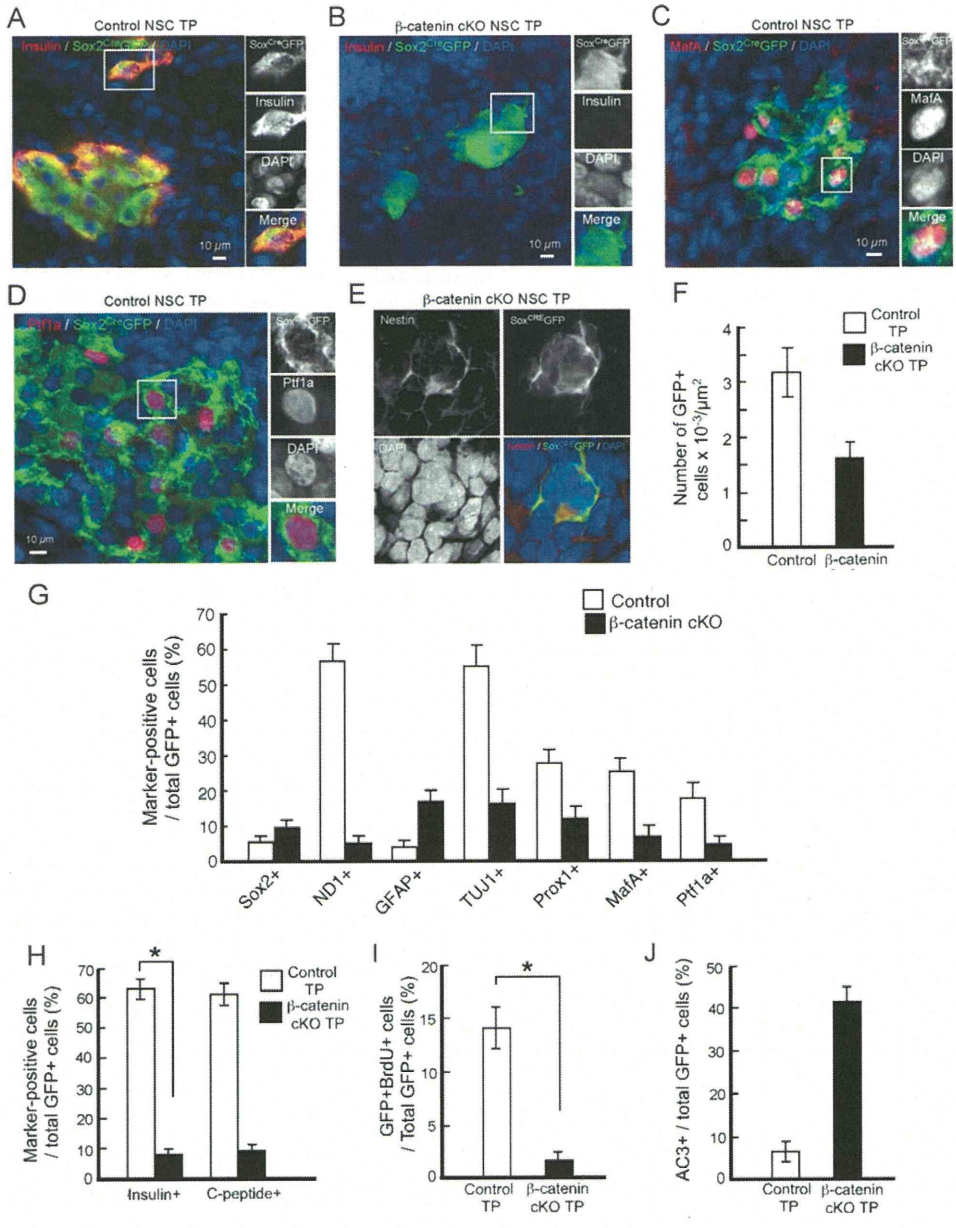

Figure 4. Transplantation of adult NSCs into the pancreas.

A. Adult HPC NSCs grafted into pancreas express insulin. IHC of tracing Sox2^{Cre}GFP cells. In control NSCs transplantation (Control NSC TP), Sox2^{Cre}GFP+ cells co-localized with insulin.

B. Adult HPC NSCs grafted into pancreas express insulin. IHC of tracing Sox2^{Cre}GFP cells. In β-catenin cKO NSCs transplantation (β-catenin cKO NSC TP), Sox2^{Cre}GFP+ cells were insulin-negative. Cells in the white square region are magnified and shown in separate panels at right. Insulin, red; Sox2^{Cre}GFP, green; DAPI, blue.

C. Detection of MafA-positive cells in grafted adult HPC NSCs into pancreas. IHC of MafA and Sox2^{Cre}GFP in control NSC TP is shown. MafA, red; Sox2^{Cre}GFP, green; DAPI, blue.

D. Ptf1a-expressing cells in grafted adult HPC NSCs into pancreas. Ptf1a, red; Sox2^{Cre}GFP, green; DAPI, blue.

E. IHC of tracing Sox2^{Cre}GFP cells in β-catenin cKO NSC TP. The β-catenin cKO NSCs remained in the nestin+ progenitor stage. Nestin, red; Sox2^{Cre}GFP, green; DAPI, blue.

F. Numbers of GFP+ cells in the pancreas of control TP mice (white bars) and β-catenin cKO NSC TP mice (black bars).

G. The phenotypic characterization of the grafted adult NSCs of control TP mice and β-catenin cKO NSC TP mice.

H. Numbers of marker and GFP double-positive cells in the grafted pancreas of control TP mice and β-catenin cKO NSC TP mice.

I. Percentages of BrdU and GFP double-positive cells in the grafted pancreas of control TP mice and β-catenin cKO NSC TP mice.

J. Numbers of AC3 and GFP double-positive cells in the grafted pancreas of control TP mice and β-catenin cKO NSC TP mice.

Adult HPC and OB NSCs were prepared from type I (STZ-induced DB rats) and type II DB rats (GK/slc DB rats) and were transplanted back into the pancreases of type I and type II DB rats, respectively. During 2 weeks *ex vivo* culture of NSCs, insulin expression was examined following Wnt3a and anti-IGFBP-4 addition. Although the HPC of DB animals contained higher IGFBP-4 and lower Wnt3 levels than wild-type (Fig 2D), Wnt3a and anti-IGFBP-4 treatment during the *ex vivo* culture rescued insulin expression (Fig 5A). These HPC and OB NPs were infected with a retroviral CAG promoter-driven EGFP expression vector to trace the grafted cells (Zhao et al, 2006). GFP+ NPs were transplanted into the pancreas of 8-week-old DB rats. Three to five collagen sheets were stacked and grafted near the splenic lobe among the three pancreatic lobes (i.e. the splenic, gastric and duodenal lobes, $n = 8$ *per* group), and blood glucose levels were recorded. Seventeen weeks after the transplantation, rats were injected with BrdU daily for 10 days.

The blood glucose levels of GFP-labelled HPC NP DB and OB NP DB transplants on collagen sheets were significantly reduced (Fig 5B and Fig S8F of Supporting information) and accompanied by up-regulated plasma and pancreatic insulin levels (Fig S8D and E of Supporting information). Nineteen weeks after transplantation, grafted OB NP DBs were insulin+ (Fig 5C, white arrows indicate GFP+ insulin+ grafts, and the arrowhead indicates an endogenous islet expressing low levels of insulin). We removed stacked cell sheets from splenic lobes 15 or 19 weeks after transplantation (Explant; Fig 5B and Fig S8F of Supporting information) to verify that the grafted GFP NPs were solely responsible for reducing blood glucose levels. We found that blood glucose levels increased ($n = 4$ *per* group of explant surgery), demonstrating that the grafted NPs produced insulin in DB rats.

To determine whether grafted adult NPs contributed to regulating glucose metabolism, we compared the animals' responses to glucose by measuring blood glucose level kinetics after transplantation. Animals transplanted with HPC NP DB and OB NP DB efficiently cleared glucose (Fig 5D). Furthermore, GFP+ cells expressing insulin were labelled by BrdU (Fig 5E), suggesting that the grafted cells proliferated. These data indicated that regulated insulin secretion by the grafted adult NPs from DB HPC and OB contributed to glucose homeostasis in the host DB rats.

DISCUSSION

Redundancy is a key feature of evolution that enables the conservation of efficient mechanisms; the most common manifestation of redundancy is exemplified by proteins that serve multiple purposes within the same cells at different developmental stages or in different cell types or tissues. Our analysis revealed that adult NSCs became insulin+ in the adult brain and in NSC-injected pancreas. The grafted NSCs reduced blood glucose and up-regulated insulin levels. NPs derived from OB and HPC produced insulin functionally via the support of Wnt3 (Fig 5). In embryonic pancreatic development, GFAP expression, representing the α cell population, was observed in cells derived from embryonic day 11 (E11) murine pancreatic buds (Fig S9A of Supporting information, left panel), where no TUJ1-positive cells, representing a β cell population, were detected. This indicated dominant α cell generation. In E17, TUJ1-positive cells (β cells), were generated on the α cell layer (Fig S9A of Supporting information, right panel), indicating that α cell generation preceded β cell generation in pancreatic development. In contrast, most cells derived from E11 murine brain stained positive for TUJ1 (Fig S9B of Supporting information, left panel). GFAP expression was restricted almost completely to the E11 brain, indicating that neuronal cell generation predominated, consistent with another report (Namihira et al, 2009). In E17, both TUJ1- and GFAP-positive cells were found (Fig S9B of Supporting information, right panel). Delayed gliogenesis in the embryonic brain has been demonstrated to result from methylation of the *GFAP* promoter (Takizawa et al, 2001). ChIP analysis indicated that GFAP expression responded to LIF stimulation (Nakashima et al, 1999) in E11 pancreatic buds but not in the E11 embryonic brain (Fig S9D of Supporting information). In E17, GFAP promoter methylation was detected at low levels in both the embryonic brain and pancreatic buds (Fig S9C of Supporting information). In adults, restricted GFAP expression was not observed in either HPC or pancreas (Fig S9C and D of Supporting information). These data suggest that the regulatory mechanisms that create Wnt3-secreting astrocyte or α cell niches are similar in the pancreas and HPC, at least in the adult stages, whereas, embryonic lineage commitment differs.

Our present study also suggested that the balance between the stimulatory actions of Wnt3 and the inhibitory actions of IGFBP-4 was regulated by DB status. IGFBPs modulate bioactivities of IGFs (Firth and Baxter, 2002), and IGF-1 and IGF-2 have been suggested to stimulate pancreatic islet cell growth (Le Roith, 2003; Liu, 2007). In the adult HPC, insulin/IGF expression facilitates NSC differentiation into the oligodendrocyte lineage (Hsieh et al, 2004) and enhances neuronal survival (Cheng and Mattson, 1992; Doré et al, 1997; Lindholm et al, 1996). IGF overexpression in transgenic mice results in brain enlargement and an increase in its myelin content (Carson et al, 1993; Ye et al, 1995). IGFs attenuate IGFBP-4 function when exogenously supplied to differentiating cardiomyocytes (Zhu et al, 2008). In diabetes, IGF-1 and IGF-2 were down-regulated along with *Wnt3* in both adult HPC and the pancreas (Fig 2C and D). These findings suggest that IGFBP-4 competitors (IGF-1 and IGF-2) were down-regulated in diabetes. Under normal conditions, insulin was expressed with the help of Wnt3, although IGFBP-4 was present. We hypothesize that endogenously expressed IGF-1 and IGF-2 control IGFBP-4 under normal conditions in both tissues. However, when DB status proceeds to a point where up-regulated IGFBP-4 and reduced IGF-1 and IGF-2 are observed, each factor likely further inhibits Wnt3-mediated signal transduction.

NeuroD1 is among the critical target genes of Wnt/β-catenin signalling in the adult stage. Sox2+ adult NSCs cannot express insulin when Wnt/β-catenin signalling is blocked endogenously (Fig 4), since adult NSCs with deleted *β-catenin* cannot trigger *NeuroD1* expression. The deletion of *NeuroD1* in adult HPC

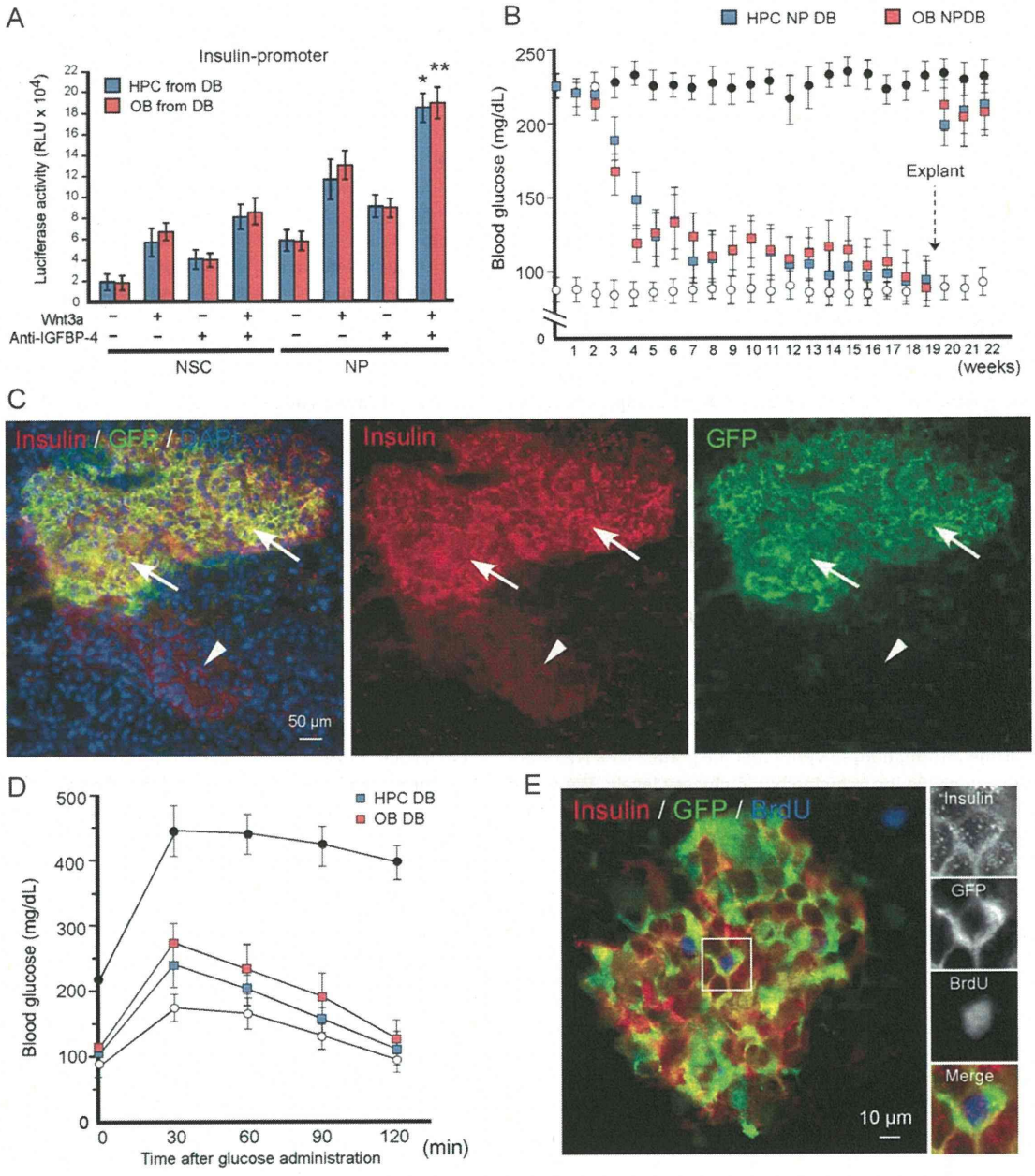

Figure 5. Therapeutic treatment of diabetes by adult NSC transplantation.

A. Insulin expressions in HPC and OB NSCs derived from DB rats. Insulin promoter activity was measured by using the luciferase reporter construct in adult HPC and OB NSC cultures that were prepared from type II DB rats [GK/slc rats, male; HPC from DB (blue bars) and OB from DB (red bars)]. The effect of Wnt3a ligand and anti-IGFBP-4 on the reporter was assessed in both undifferentiated NSCs and the NP cells. $^{*}p < 0.01$ and $^{**}p < 0.001$.

B. The effect of the grafted adult NPs in DB animals. HPC and OB NPs from type II diabetes rats were prepared *ex vivo* under treatment with Wnt3a and anti-IGFBP-4, and the resultant HPC NP DB and OB NP DB were transplanted into the pancreas of diabetes rats. Open circles, normal rats control; blue squares, HPC NP DB; red squares, OB NP DB; closed circles, diabetes GK/slc rats.

C. IHC of tracing CAG promoter driven EGFP cells (OB NP DB) in type II GK/slc DB rats. Co-localizing cells for insulin and GFP are indicated by white arrows. The preexisting islet expressing insulin at lower levels is indicated by the white arrowhead. Insulin, red; CAG-GFP, green; DAPI, blue.

D. Average of blood glucose levels in the response to intraperitoneal glucose tolerance test. Eighteen weeks after the implantation of adult NPs into rat pancreas, blood glucose levels were measured to glucose administration. Open circles, wild-type rats; blue squares, HPC NP DB grafts into DB rats; red squares, OB NP DB grafts into DB rats; closed circles, GK/Jcl DB rats. $n = 4$ *per* each group.

E. IHC of tracing HPC NP DB cells in DB rats. Cells in the white square region are magnified and shown in separate panels at right. Insulin, red; CAG-GFP (GFP), green; BrdU, blue.

results in decreased survival and maturation of newborn neurons (Gao et al, 2009). The diabetes-dependent impairments of adult hippocampal neurogenesis and synaptic plasticity might result from the diminished Wnt signalling that leads to *NeuroD1* down-regulation. Because *NeuroD1* is important for activating insulin mRNA expression, the decline in Wnt/β-catenin signalling in diabetes may impair *de novo* insulin mRNA expression by attenuating *NeuroD1* expression.

Our present study revealed that adult HPC and OB NSCs possess the intrinsic ability to generate insulin-producing cells via Wnt/β-catenin signalling. Since the successful isolation of NSCs from human adult OB was first reported, OB NSCs have attracted considerable attention as an accessible source of NSCs for studying various diseases. Adult HPC and OB NSCs derived from DB animals retained the ability to produce insulin in *ex vivo* culture (Fig 5). We further determined that the best source of insulin supply for transplantation into DB animals was adult NPs that had been committed into early neuronal lineage and had been treated with anti-IGFBP4 and Wnt3a to rescue their impaired Wnt signalling in DB animals. Grafted adult HPC and OB NPs reduced blood glucose levels for more than 2 months in DB rats (Fig 5B).

Various cell-based approaches have been explored for diabetes treatment: (1) differentiation to the β cell lineage from embryonic stem cells and/or induced pluripotent stem cells (iPS cells) (Lumelsky et al, 2001; Tateishi et al, 2008; Zhang et al, 2009), (2) direct conversion of differentiated cells into β cells (Thorel et al, 2010; Zhou et al, 2008) and (3) trans-differentiation of adult progenitor cells (Seaberg et al, 2004). This study provides an example of the direct use of adult stem cells from one organ to another without introducing inductive genes. Using adult NSCs for treating diabetes is potentially advantageous because donors are not required, the introduction of inductive genes is not necessary, and extracellular and endogenous regulation suitably resembles that employed by adult islet endocrine cell lineages. Although further studies, including the validation of other adult NSCs, should be forthcoming, the basic strategy outlined here should be useful for preliminary treatment of diabetes using the patient's own NSCs before the disease progresses.

MATERIALS AND METHODS

Cell preparation and culture

Female 7- to 8-week-old Fisher 344 rats with a body weight of 100–150 g were used (Charles River Japan, Inc). All animal procedures were performed according to a protocol approved by the Institutional Animal Care and Use Committee (IACUC) of the National Institute of Advanced Industrial Science and Technology. Adult NSCs were prepared and maintained as described previously (Dictus et al, 2007; Gage et al, 1995). The studies are described in more detail in the Supporting information.

In situ hybridization

Brains were dissected from freshly euthanized Fisher 344 rats and put in ice-cold saline until blocking. Brains were then placed in plastic blocks in insulin OCT (TissueTek) and frozen. Sections were cut at 15 μm by cryostat (LEICA CM1850. Leica). Brain sections on the slide-glass were hybridized with labelled riboprobes as described in more detail in the Supporting information.

Enzyme-linked immunosorbent assay of insulin

The insulin content of brain, HPC, femoral muscle, pancreatic head and pancreatic tail was measured by ELISA. Liquid nitrogen snap-frozen tissues of each age (7-week-old and 16-month-old Fisher 344 rats) were immediately homogenized and immunoreactive insulin was determined using rat insulin ELISA kit (Shibayagi, Gunma, Japan) according to the manufacturer's protocol: For details, see the Supporting information.

DNA Microarray

Total RNA from HPC/OB was extracted using ISOGEN (NipponGene) and labelled with Cy3. Samples were hybridized with Whole Rat Genome Microarray (G4131F, Agilent). Each sample was hybridized with the one colour protocol. Arrays were scanned with a G2505C Microarray Scanner System (Agilent). Data analysed by using GeneSpring GX11.0 software (Agilent). Two normalization procedures were applied; first, signal intensities less than 1 were set to 1. Then each chip was normalized to the 75th percentile of the measurements taken from that chip. Baseline transformation of those data did not perform. Genes with 'present' and 'marginal' flag value in all samples were used for analyses (32,622 genes). GO terms enriched with *p*-value cut off of 0.1 are extracted. The raw microarray data were submitted to the Gene Expression Omnibus (GEO) microarray data archive (http://www.ncbi.nlm.nih.gov/geo/) at the NCBI (accession numbers GSE27956).

Immunohistochemical analysis (IHC)

Immunofluorescence studies were primarily performed as described previously (Kuwabara et al, 2009): mouse monoclonal-beta tubulin-III (TUJ1; 1:500; Promega), guinea pig anti-insulin (1:300; Sigma), goat anti-C-peptide (1:250; Linco Research), goat anti-NeuroD (1:100; Santa Cruz), guinea pig anti-GFAP (1:500; Advanced Immunochemical Inc.), mouse anti-glucagon (1:300; Immuno), goat antibody to Wnt3 (1:100, Everest), mouse antibody to nestin (BD Biosciences), rat anti-BrdU (1:250; Abcam) and DAPI (Wako). All secondary antibodies were obtained from Jackson ImmunoResearch. The images were analysed using a Carl Zeiss LSM confocal imaging system (LSM 510; Carl Zeiss, Tokyo, Japan) or Olympus FV1000-D confocal microscope (Olympus Corporation, Tokyo, Japan).

Microscopic analysis and quantification

Microscopic analysis and quantification were completed as previously described (Kuwabara et al, 2009). Slides were coded during IHC analysis, and the code was not broken until after analysis was complete. Briefly, quantification of cell number within the DG of HPC was performed using the 20X objective of a Carl Zeiss LSM confocal imaging system (LSM 510; Carl Zeiss) or Olympus FV1000-D confocal microscope (Olympus Corporation) by an observer blind to experimental groups. Wnt3+, Insulin+, GFP+, BrdU+ and AC3+ cell quantification and morphology phenotyping were completed in every 12th 40-μm coronal section throughout the SGZ and outer portion of the GCL of the DG (bregma, −0.80 to −4.20 mm). Phenotypic analysis and co-localization of GFP+ cells with various markers in the DG were

The paper explained

PROBLEM:

The number of patients receiving care for type 1 and type 2 diabetes has more than doubled since the past decade. In type 1 diabetes, the patient's immune system aberrantly destroys the insulin-producing β cells of the pancreas. Type 2 diabetes is caused by insulin resistance, progressively reaching the point where β cells can no longer produce enough additional insulin. Cell replacement therapy can be an effective strategy to treat diabetes; however, insufficient supply of β cells from human organ donors is a major issue. Using stem cells as a potential source for deriving new β cells in a safe and easy way has long been awaited for.

RESULTS:

We demonstrated that subpopulations of neurons and adult NP cells express insulin in the brain. Adult NSCs, derived from the HPC and OB, give rise to insulin expressing cells. Adult NPs from DB rats could still generate insulin-producing cells, and the process requires the activation of NeuroD1 transcription factor via Wnt3 signalling. Under normal circumstances, insulin-expressing cells of neuronal lineage do not express phenotypic markers of pancreatic β cells. However, after transplantation into the pancreas, these neuronal cells not only increase their production of insulin but also start to express several transcription factors characteristic for pancreatic beta cells. As an approach to stem cell therapy that could be applied without gene transfer techniques, we supplied adult NPs from DB rats into the pancreases of DB rats. We found that this treatment induced insulin expression, reduced blood glucose levels and up-regulated insulin levels. Removal of these implants led to elevated levels of blood glucose, indicating that transplanting neural progenitor/stem cells into the pancreas could be a useful approach for treating diabetes.

IMPACT:

Our data indicate that adult NSCs are a relevant and safe cell source of insulin-producing cells. OB-derived NSCs are particularly useful because of their easily accessible location and their ability to generate insulin-producing cells, as hippocampal NSCs do. The findings of this study indicate the potential value of this technique for treating human diabetes without gene transfer, and would contribute as a novel strategy to overcome donor issues in cell replacement therapy of diabetes.

done on randomly assigned coronal sections throughout the SGZ using a confocal microscope (Carl Zeiss LSM confocal imaging system; 40X objective). Carl Zeiss Confocal Software was used for scanning, optical sectioning in the Z plane and 3D rendering.

Chromatin immunoprecipitation (ChIP) and qRT-PCR

ChIP was performed essentially according to the manufacturer's protocol by using a commercial kit (Upstate). Briefly, DNA was cross-linked to protein with formaldehyde. Cellular lysate was obtained by scraping, followed by pulse ultrasonication to shear cellular DNA. Immunoprecipitations were performed with 1.0 μg of antibodies and bound DNAs were purified by phenol:chloroform extraction. Resultant purified DNAs were analysed using quantitative PCR as described above. For details, see the Supporting information.

Animals

For the IHC analysis, we used 8- to 10-week-old C57/BL6 mice, 7- to 12-week-old adult female Fisher 344 rats, 3- to 4-week old young adult Fisher 344 rats, GK/slc type II DB rats and STZ- (70 mg/kg injectable dose; Wako) induced diabetic Fisher 344 rats (Type I diabetes model; 10-week-old females). The studies are described in more detail in the Supporting information.

Statistics

Experiments were analysed for statistical significance using a Student's *t* test, with all error bars expressed as ± standard error of mean (s.e.m.). Values of $p < 0.05$ or $p < 0.001$ were considered significant.

Author contributions

TK, MNK, FHG and MA conceptualized and designed the experiments; TK, MNK, YO, YI, MW and KT did the experiments; TK, MNK, YI, TS, KN and FHG analysed the data and prepared the manuscript.

Acknowledgements

We thank Takahisa Ohtake, Takahiro Numabe and Hideto Takimoto for providing assistance in the care of animals and in the experiments. We thank Mary Lynn Gage for editorial comments. TK, YO, YI, MW, KT and MA were supported by various grants from AIST. TK was partly supported by Suzuken memorial foundation and the Grant-in-Aid for Young Scientists (B). KN and TS were supported by the Foundation for Nara Institute of Science and Technology.

Supporting information is available at EMBO Molecular Medicine online.

The authors declare that they have no conflict of interest.

For more information

SCRC web page:
http://unit.aist.go.jp/scrc/cie/index_en.html